

THESIS FOR THE DEGREE OF DOCTOR OF PHILOSOPHY

Experimental and kinetic studies of H₂ effect on lean
exhaust aftertreatment processes: HC-SCR and DOC

MUHAMMAD MUFTI AZIS



Department of Chemistry and Chemical Engineering

CHALMERS UNIVERSITY OF TECHNOLOGY

Göteborg, Sweden 2015

Experimental and kinetic studies of H₂ effect on
lean exhaust aftertreatment processes: HC-SCR and DOC
Muhammad Mufti Azis
ISBN: 978-91-7597-170-4

© MUHAMMAD MUFTI AZIS, 2015

Doktorsavhandlingar vid Chalmers tekniska högskola
Ny serie nr. 3851
ISSN 0346-718X

Cover: The picture illustrates the concept of utilizing H₂ to improve DOC and HC-SCR performances on lean exhaust aftertreatment processes.

Department of Chemistry and Chemical Engineering
Chalmers University of Technology
SE-412 96 Göteborg, Sweden
Telephone +46 (0)31 772 1000

Printed by:
Chalmers Reproservice
Göteborg, Sweden (2015)

Experimental and kinetic studies of H₂ effect on lean exhaust aftertreatment processes: HC-SCR and DOC

MUHAMMAD MUFTI AZIS

Department of Chemistry and Chemical Engineering
Chalmers University of Technology, Göteborg 2015

Abstract

With a growing concern to lower greenhouse gas emissions from road transportation, lean burn and diesel engines will keep playing an important role in the future. Development of a highly efficient and durable process to reduce NO_x to N₂ becomes a challenging issue especially in the presence of ample O₂ concentration as in lean burn exhaust. One way to reduce NO_x emissions in lean exhaust is by using hydrocarbon-selective catalytic reduction (HC-SCR). HC-SCR over Ag/Al₂O₃ catalysts appears to be a promising technology to abate NO_x emission in lean burn exhaust. The function of the Diesel oxidation catalyst (DOC), as a part of a lean exhaust aftertreatment process, is to oxidize CO, HC and NO. Interestingly, addition of H₂ has been shown to promote the HC-SCR activity over Ag/Al₂O₃ and NO oxidation activity over Pt/Al₂O₃ catalyst. The overall focus of this thesis was to increase understanding of the mechanisms of the H₂ effect on the model catalysts of Ag-Al₂O₃ and Pt/Al₂O₃. A combination of experimental and kinetic modeling approaches was utilized as a way to examine mechanistic effects of H₂.

Temperature-programmed desorption (TPD) technique was used to characterize thermal stabilities of various surface NO_x species formed during NO oxidation and C₃H₆-SCR conditions over Ag/Al₂O₃ catalyst. In addition, DRIFTS analysis was used to identify different types of nitrate species. These TPD results elucidated the dual roles of H₂ to remove inhibiting nitrate on active sites and facilitate formation of inactive nitrate species mainly on the Al₂O₃ support.

An initial development of a microkinetic model to describe H₂-assisted NO oxidation over Ag/Al₂O₃ was conducted using a set of transient data. The single role of H₂ to remove inhibiting nitrate species on active sites was examined. In the further model development, a global kinetic model of H₂-assisted C₃H₆-SCR, including NO oxidation, C₃H₆ oxidation and C₃H₆-SCR in the presence and absence of H₂, was proposed. This model was based on dual roles of H₂ to remove inhibiting nitrates from active sites and simultaneously form more active Ag sites. The model could effectively capture a wide range of feed concentrations and temperatures, including temperature-programmed and transient experiments.

The influence of H₂ on NO oxidation over Pt/Al₂O₃ as a DOC catalyst was evaluated with various feed mixtures. Formation of Pt oxide has been known to lower the NO oxidation activity over Pt/Al₂O₃. The role of H₂ to retard the Pt oxide formation was investigated. This resulted in a temporal enhancement in NO₂ yield due to H₂ addition during temperature ramp experiments. In addition, the effect of C₃H₆ and CO to influence the NO oxidation was also investigated. Addition of H₂ mainly serves to weaken the inhibition effect of C₃H₆ and to a much lesser degree CO. This is mainly due to an enhancement of lower temperature C₃H₆ oxidation. The promotional effects of H₂ to increase NO₂ yield was proposed as a result of effects of H₂ on surface chemistry and/or reactions. These effects could be clearly distinguished from exothermal heat effects from mainly H₂ but also C₃H₆ and CO oxidation.

Keywords: HC-SCR, DOC, Silver Alumina, Platinum Alumina, Hydrogen effect, Kinetic modeling, NO_x reduction, NO oxidation.

List of Appended Papers

This thesis is based on the work presented in the following papers:

- I. On the role of H₂ to modify surface NO_x species over Ag-Al₂O₃ as lean NO_x reduction catalyst: TPD and DRIFTS studies**
Muhammad Mufti Azis, Hanna Härelind, Derek Creaser
Catalysis Science & Technology, 5, 2015, 296-309.
- II. Microkinetic modeling of H₂-assisted NO oxidation over Ag-Al₂O₃**
Muhammad Mufti Azis, Hanna Härelind, Derek Creaser
Chemical Engineering Journal, 221, 2013, 382-397.
- III. Kinetic modeling of H₂-assisted C₃H₆ selective catalytic reduction of NO over silver alumina catalyst**
Muhammad Mufti Azis, Hanna Härelind, Derek Creaser
Chemical Engineering Journal, DOI:10.1016/j.cej.2014.10.057
- IV. Evaluation of H₂ effect on NO oxidation over a Diesel Oxidation Catalyst**
Muhammad Mufti Azis, Xavier Auvray, Louise Olsson, Derek Creaser
submitted

Other publications not included in this thesis:

- I. On the evaluation of synthetic and natural ilmenite using syngas as fuel in chemical-looping combustion (CLC)**
Muhammad Mufti Azis, Erik Jerndal, Henrik Leion, Tobias Mattisson, Anders Lyngfelt
Chemical Engineering Research and Design, 88(11), 2010, 1505-1514.
- II. The Effect of Bituminous and Lignite Ash on the Performance of Ilmenite as Oxygen Carrier in Chemical-Looping Combustion**
Muhammad Mufti Azis, Henrik Leion, Erik Jerndal, Britt-Marie Steenari, Tobias Mattisson, Anders Lyngfelt
Chemical Engineering & Technology, 36(9), 2013, 1460-1468.

Contribution report

Paper I

I partially prepared the catalyst, performed flow reactor and DRIFTS experiments, interpreted the results together with my coworkers and was responsible for writing the manuscript.

Paper II

I prepared the catalyst, performed flow reactor experiments, performed modeling, interpreted the results together with my coworkers and was responsible for writing and submitting the manuscript.

Paper III

I prepared the catalyst, performed flow reactor experiments, performed modeling, interpreted the results together with my coworkers and was responsible for writing and submitting the manuscript.

Paper IV

I performed flow reactor experiments, interpreted the results together with my coworkers and was responsible for writing the manuscript.

Table of contents

Chapter 1. Introduction	1
1.1 NO _x emission abatement from lean-burn engine	1
1.2 Objectives and scope of the thesis	3
1.3 The outline of the thesis.....	3
Chapter 2. Diesel Oxidation Catalyst	5
2.1 General	5
2.2 NO oxidation over Pt/Al ₂ O ₃	5
2.3 H ₂ effect on DOC	7
Chapter 3. Hydrocarbon-Selective Catalytic Reduction (HC-SCR) over silver alumina catalyst	9
3.1 General	9
3.2 Silver alumina for HC-SCR	9
3.3 Mechanistic studies of HC-SCR	11
3.4 The effect of H ₂ on HC-SCR over Ag/Al ₂ O ₃	12
3.5 Onboard H ₂ production	13
Chapter 4. Experimental methods	15
4.1 Catalyst preparation: synthesis and washcoating	15
4.2 Flow reactor experiments	16
4.3 In-situ DRIFT spectroscopy	17
Chapter 5. Modeling methods	19
5.1 General	19
5.2 Kinetic modeling: global and microkinetic approaches	19
5.3 Reactor model	21
5.4 Modeling of mass balance	22
5.5 Modeling of heat balance	23
5.6 Matlab implementation: simulation and parameter estimation	23

Chapter 6. Stability of surface NO_x species: TPD and DRIFTS studies	25
6.1 Roles of surface NO _x species	25
6.2 TPD studies of NO _x	25
6.3 Stability of surface NO _x species from in-situ DRIFT Spectroscopy.....	28
6.4 Mechanistic insight regarding C ₃ H ₆ -SCR and H ₂ -assisted C ₃ H ₆ -SCR	29
Chapter 7. Kinetic studies of the H₂ effect on NO oxidation and C₃H₆-SCR over Ag-Al₂O₃	33
7.1 General	33
7.2 Microkinetic modeling of H ₂ -assisted NO oxidation (Paper II)	33
7.3 Kinetic modeling of H ₂ -assisted C ₃ H ₆ -SCR (Paper III)	37
Chapter 8. Surface species quantification as a support for SCR model	45
8.1 Experimental estimation of surface NO _x species using TPD technique	45
8.2 Interpretation of surface NO _x species to give insights for mechanistic study	47
Chapter 9. Evaluation of the H₂ effect on DOC	49
9.1 The effect of H ₂ with various gas mixtures	49
9.2 The effect of H ₂ to influence hysteresis	51
9.3 Transient NO ₂ yields at constant temperature	52
9.4 Transient experiments with in/out H ₂ switching	52
9.5 Discrimination of heat and chemical effects due to addition of H ₂	54
9.6 Influence of H ₂ on Pt oxide formation	55
9.7 H ₂ influence on C ₃ H ₆ and CO oxidation and interactions with NO oxidation	56
Chapter 10. Conclusions and outlook	59
Acknowledgements	62
References.....	63

List of abbreviations

AIP	Aluminium isopropoxide
APU	Auxiliary power unit
ATR	Autothermal reformer
BET	Brunauer–Emmett–Teller
BOC	Bond-order conservation
CPSI	Cells per square inch
DAE	Differential algebraic equations
DFT	Density functional theory
DOC	Diesel oxidation catalyst
DOE	Design of experiment
DME	Dimethyl ether
DPF	Diesel particulate filter
DRIFTS	Diffuse reflectance infrared fourier transform spectroscopy
E85	Ethanol fuel blend of 85% denatured ethanol fuel and 15% gasoline
EGR	Exhaust gas recirculation
FTIR	Fourier transform infrared
FTP	Federal test procedure
GHSV	Gas hourly space velocity
HC	Hydrocarbon
HT	High temperature
ICE	Internal combustion engine
IR	Infrared
LNT	Lean NO _x trap
LT	Low temperature
MLR	Multi-linear regression
MS	Mass spectrometer
NSR	NO _x storage and reduction
PGM	Platinum group metal
SCR	Selective Catalytic Reduction
SSE	Sum of squared errors of prediction
TPD	Temperature-programmed desorption
TPR	Temperature-programmed reaction
UBI-QEP	The unity bond index-quadratic exponential potential
VOC	Volatile organic compounds
WHSV	Weight hourly space velocity

Nomenclature

Roman symbols	Description	Unit
A	mass and/or heat transfer area	m^2
A_i	pre-exponential factor	s^{-1}
C	concentration	$mol.m^{-3}$
cp	heat capacity	$J.mol^{-1}.K^{-1}$
$Deff$	effective diffusivity	$m^2.s^{-1}$
Ea	activation energy	$kJ.mol^{-1}$
F_{tot}	molar flow rate	$mol.s^{-1}$
h	convection heat transfer coefficient	$J.m^{-2}.K^{-1}$
ΔH_R	enthalpy change of overall gas reaction	$J.mol^{-1}$
k	rate constant	s^{-1}
Keq	equilibrium constant	-
kc	mass transport coefficient	$m.s^{-1}$
$\ln(k_{ref})$	natural logarithmic of rate constant at ref. temperature	$mol.s^{-1}.kg^{-1}$
N_c	number of sites	$mol.kg^{-1}$
r	reaction rate	$mol.s^{-1}.kg^{-1}$
$range$	range for parameter scaling	-
R	gas constant	$J.mol^{-1}.K^{-1}$
ΔS_R	entropy change of overall gas reaction	$J.mol^{-1}.K^{-1}$
t	time step	s
T	temperature	K
w	mass of segmental catalyst	kg
ΔX	thickness of segmental layer	m
y	molar fraction	-

Greek symbols	Description	Unit
β	fitted kinetic parameters	-
Γ	lumped mass transfer coefficient	$m^3.s^{-1}$
θ	fractional surface coverage	-
ν	stoichiometric coefficient	-
χ	stoichiometric coefficient of adsorbed species	-

Subscript	Description
b	backward reaction
f	forward reaction
g	gas
i	gas component index
j	reaction index
k	tank index
n	layer index
ref	reference condition
s	solid
w	surface component index

Chapter 1

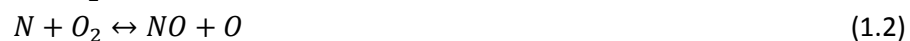
Introduction

1.1 NO_x emission abatement from lean-burn engine

Improvement of urban air quality is always an important environmental issue particularly with a growing concern to create a sustainable society. Road transportation is a major contributor to urban air pollution and therefore regulations have been made in several countries to reduce emissions from road transportation such as the Clean Air Act in the US and European emission standard EURO. The major air pollutants targeted in the regulations are CO, Nitrogen oxide (NO_x), Hydrocarbon and particulate matter [1]. Since global warming is also an alarming concern nowadays, very recently greenhouse gases emissions (notably CO₂) from vehicles have also been regulated for light duty and heavy duty fleets [1, 2].

NO_x is an interesting and important air pollutant. Its occurrence in the atmosphere is due to exhaust gas produced in combustion engines, which is the most common form of propulsion for vehicles [3]. Emission of NO_x to the atmosphere has severe consequences. Firstly, NO_x plays a crucial role in the acid deposition problem [4]. In the atmosphere, NO readily oxidizes to NO₂ (reddish brown gas) and NO₂ reacts further with water vapor to form nitric acid and cause acid deposition (acid rain) that damages trees, soils and lakes. Secondly, NO together with NO₂ are responsible for the formation of photochemical smog. Nitrogen oxides reacts with sunlight and volatile organic compounds (VOC) to form air-borne particles and ground level ozone known as photochemical smog. Smog usually occurs in large cities with sunny and warm climates packed with heavy road traffic. Photochemical smog has also serious health effects as it may cause or exacerbate respiratory related diseases [3, 4].

Most Internal combustion engines (ICE) nowadays use fossil fuel and compressed air. Since air contains 79% N₂, in a highly oxidative atmosphere N₂ can be converted to NO_x. The so called thermal NO_x is produced from equilibrium reactions between N₂ and O₂ at elevated temperatures such as in an ICE. Thermal NO_x is conceived as the major contributor of NO_x formation from conventional diesel engines which primarily consists of NO (70-90% of total NO_x). The mechanism of NO formation is described by the *extended Zeldovich mechanism*[3, 5]:



There are also minor routes for NO_x formation originating from prompt NO and fuel nitrogen [5].

In the late 70s, the commercial three way catalyst was introduced in the US and functioned effectively to reduce CO, hydrocarbon and NO_x emissions in parallel from gasoline engines. In an ordinary gasoline engine, the ratio between the air and fuel is near stoichiometric conditions for complete combustion. In line with the demand to achieve better fuel efficiency, diesel engines or lean-burn engines will increasingly become the major type of combustion engine in the future. In a diesel engine or lean-burn engine, the O_2 supply (as air) is in excess with respect to the amount of fuel and this will result in improved power output with lower CO_2 emissions [1, 6]. However, the conventional three way catalyst does not function effectively to remove emissions from the lean-burn exhaust, particularly NO_x emissions. Therefore, improved designs of vehicle emission abatement system for lean exhaust are continuously being designed and implemented [6].

There are two broad methods to control NO_x emissions from ICE: pollution prevention aiming to reduce NO_x generation (primary technique) and post-combustion treatment aiming to reduce NO_x emissions (secondary technique) [3]. In a primary technique, NO_x generation in the ICE is suppressed by decreasing combustion temperature and controlling the oxygen-fuel concentration. An example of a primary technique is Exhaust Gas Recirculation (EGR). Selective catalytic reduction is an example of a secondary NO_x abatement method.

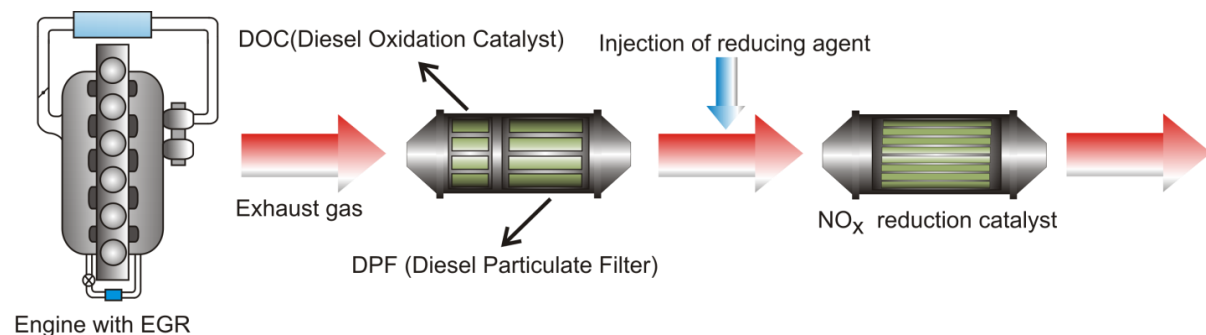


Figure 1.1 General schematic view of aftertreatment system in a lean-burn or diesel engine vehicle

A catalytic aftertreatment system is a common method to abate vehicle emission from mobile sources. For a modern diesel engine, the catalytic aftertreatment system often consists of three primary parts: diesel oxidation catalyst (DOC), diesel particulate filter (DPF) and NO_x reduction catalyst as depicted in Figure 1.1. The main function of the DOC is to oxidize carbon containing species and to oxidize NO to NO_2 . In the following part, the DPF traps solid particulate matter and NO_2 produced upstream in the DOC can be used for passive regeneration of the DPF. Eventually, a NO_x catalyst is installed to convert the NO_x to N_2 before releasing it to the atmosphere.

For NO_x reduction in a lean-burn system, Selective Catalytic Reduction (SCR) is a reliable method and has been widely installed in both mobile and stationary systems. With the SCR technique, the NO_x is converted to N₂ with the aid of reductants. One way to do this is by using NH₃ (or urea solution) as the reducing agent, so called NH₃-SCR. Additional installation of a urea tank is needed onboard and it further requires an injection strategy to achieve better efficiency in NH₃ consumption.

Another technology to catalytically reduce NO_x is the lean NO_x trap (LNT) pioneered by Toyota which appeared on the market in 1994 [7]. Here, the NO_x is stored on a catalyst (typically a Barium based catalyst) under a lean period that is followed by a short period of rich operation to regenerate the catalyst using a reducing agent. One of the challenges in LNT is deactivation by sulphur poisoning, where sulphur is converted to strongly bound sulphates and thus decreases the NO_x storage capacity (as nitrates). Several attempts to improve the LNT technique have been discussed in literature [8].

The third concept of de-NO_x technology in a lean-burn engine is hydrocarbon-SCR (HC-SCR). Here, the goal is to use the diesel fuel itself as a reducing agent and therefore installation of an additional tank for a reducing agent is not required. One of the potential catalysts for HC-SCR is silver alumina. Since studies of HC-SCR over silver alumina catalysts will comprise a large part of this thesis, it merits further discussion as presented in the following chapter.

1.2 Objectives and scope of the thesis

The overall goal of the project is to increase understanding of the reaction mechanisms of the H₂ effect on HC-SCR and DOC from lab-scale studies. For this purpose, both experimental and modeling approaches were used. Two types of catalyst were used: Ag-Al₂O₃ and Pt/Al₂O₃ to represent a HC-SCR catalyst and DOC, respectively. As indicated by the distribution of publications appended to this thesis, a larger portion of the thesis is allocated for HC-SCR than DOC studies.

In this thesis, a large portion of the experimental studies were based on activity measurements using monolithic samples and flow reactor facilities. Temperature-programmed reactions as well as transient tests have been used widely to understand the H₂ effect on both HC-SCR and DOC. Some of the data were then used to assemble kinetic models for mechanistic studies. In addition, temperature-programmed desorption (TPD) and DRIFT Spectroscopy were also used to facilitate the development of mechanistic models.

1.3 The outline of the thesis

This thesis is divided into 10 chapters and the highlights of each chapter are presented here. **Chapter 1** is intended to present a general overview and the objective of this thesis. **Chapter 2** deals with a brief literature review on DOC particularly related to the characteristics of the NO oxidation reaction. **Chapter 3** presents a literature review on HC-SCR over silver alumina, reaction mechanisms and H₂ promotional roles. Subsequently, experimental methods used in the present work are presented in **Chapter 4**. **Chapter 5** gives an overview of the kinetic

and reactor model used in the present work. **Chapter 6** summarizes **Paper I** by describing the H₂ role to modify surface NO_x species in the framework of HC-SCR. **Chapter 7** summarizes **Paper II** and **Paper III** related to the mechanistic modeling studies of the H₂ effect on NO oxidation and C₃H₆-SCR. **Chapter 8** contains results from surface species quantification to support C₃H₆-SCR kinetic model. **Chapter 9** summarizes an evaluation of the H₂ effect to enhance NO oxidation over Pt/Al₂O₃ (**Paper IV**). Eventually, **Chapter 10** presents concluding remarks of this thesis and an outlook for future work.

Chapter 2

Diesel Oxidation Catalyst

2.1 General

The function of the Diesel Oxidation Catalyst (DOC) is to oxidize CO, HC and soluble organic fractions in particulate matter [9]. In addition, the DOC also facilitates oxidation of NO to NO₂. It has been widely reported in the literature that the presence of NO₂ from the outlet stream of the DOC is not only beneficial to enhance oxidation of trapped particulate matter in the subsequent DPF unit, but also favorable for the fast SCR reaction over the NH₃-SCR unit (the common type of current technology for NO_x removal). As shown in Figure 1.1, DOC is typically placed as the first catalyst to process the exhaust gases due to its oxidative functionality. For this purpose, noble metal based catalysts containing Pt and Pd are commonly employed as the main components in a DOC. When appreciable amounts of sulphur are present in the fuel, it may invoke deactivation of the DOC and facilitate formation of undesired sulphate PM by the DOC. Undesired oxidation of SO₂ in the DOC may also invoke H₂SO₄ formation. Subsequently, interaction between H₂SO₄ and water vapor leads to crystallization of sulphate components known as sulphate particulates [9, 10]. This process contributes to an increase in the PM emissions from the outlet DOC stream.

2.2 NO oxidation over Pt/Al₂O₃

Considering the beneficial effects of NO₂ formation as addressed earlier, kinetic studies of NO oxidation over the DOC have been widely reported in literature, e.g. a DOC review by Russell et al. [11]. Other than for the DOC application, NO oxidation is also known to be one of the primary steps of the lean NO_x trap (LNT) application. As a result, considerable attention on NO oxidation studies has also been reported for conventional LNT catalysts, Pt/BaO/Al₂O₃ e.g. in [12, 13]. NO oxidation in the lean exhaust atmosphere over Pt/Al₂O₃ exhibits some interesting features that can be summarized by the following points:

- At high temperature, the activity for NO oxidation is typically limited by thermodynamic equilibrium. It is also worth noting that the reaction is self-inhibited by the produced NO₂.

- During temperature-programmed oxidation, hysteresis phenomenon for NO oxidation conversion is commonly observed where the activity during the cooling ramp is usually lower than the preceding heating ramp.
- The NO oxidation reaction is also ascribed to be a structure-sensitive reaction.
- Related to its interaction with other compounds like CO and HC, it has been found that NO, CO and HC inhibit each other for their oxidations.

Due to the thermodynamic limitation at high temperature, the DOC is expected to have optimal performance in the medium-high temperature range. An example of NO oxidation activity over Pt/Al₂O₃ catalyst during a heating and subsequent cooling ramp is shown in Figure 2.1 where the hysteresis of NO oxidation is clearly shown. The hysteresis phenomenon on the DOC is generally explained by formation of Pt oxide facilitated by O₂ and NO₂ [13-15]. The build-up of Pt oxide with time which deactivates NO oxidation has also been widely studied in literature [12, 13].

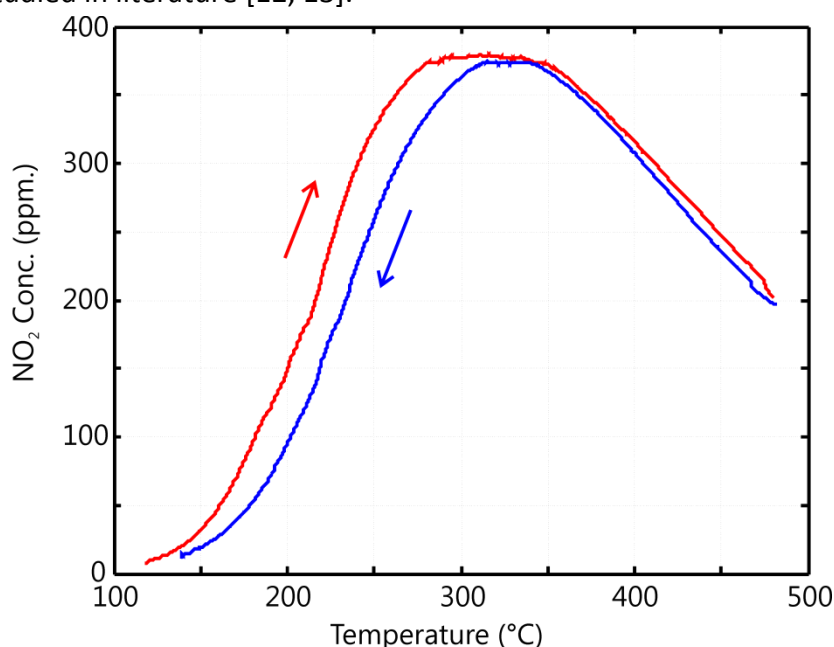


Figure 2.1 Hysteresis behavior of NO oxidation activity over 1 wt.% Pt/Al₂O₃ catalyst with ramping rates of $\pm 5^\circ\text{C}/\text{min}$. Inlet feed: 500 ppm NO, 8% O₂, 5% H₂O and Ar balance.

Since NO oxidation is a structure sensitive reaction, a number of studies have been conducted to relate the effect of Pt particle size/morphology on NO oxidation. Pt dispersion (particle size) has been reported to have a more important role than support materials [16]. Interestingly, it has been shown that larger particle size is beneficial for NO oxidation [16, 17]. This has been attributed to a higher resistance of large particles against Pt oxide formation by weakening the Pt-O bond [18]. Aging treatments have also been reported as a way to modify the Pt particle size [17]. The presence of O₂ in the gas composition during an aging treatment is beneficial as it further increased the NO oxidation conversion. This was proposed to be due to less Pt oxide formation and better ability to dissociate O₂ during adsorption step which is often regarded as the rate limiting step in NO oxidation [17, 19].

The interaction of CO, HC and NO on the oxidation of each component is already presented in literature e.g. in [20]. The presence of HC was found to inhibit NO oxidation and can be ascribed to competitive adsorption on the oxidation sites or reduction of NO₂ to NO due to reaction with HC [11]. Similarly, CO was found to inhibit NO oxidation in the same manner as HC i.e. competitive adsorption and NO₂ reduction to NO by CO [15, 20]. The inhibition of CO and HC on NO oxidation disappeared as the temperature increased, approaching the light-off temperature for CO or HC oxidations. Hauff et al. [15] reported that in NO/CO mixtures following complete conversion of CO, the NO oxidation conversion is higher than in the absence of CO. This is proposed due to the ability of CO to block the surface at low temperature and thus prevent Pt oxidation to occur. Related to the role of CO to retard Pt oxide formation, increasing CO concentrations has also been reported to improve NO oxidation conversion on a Pt/TiO₂ catalyst [21].

2.3 H₂ effect on DOC

Addition of H₂ in real diesel exhaust gas, as a way to improve oxidation activity over Pt and Pt-Pd DOC catalysts, has been reported by Herreros et al.[22]. As a result, improvements in NO₂ yield as well as higher CO and HC conversion were obtained. Only a portion of this promotional effect was found to stem from the temperature rise due to H₂ oxidation. Due to the complex gas composition of real diesel exhaust, it is challenging to investigate the intrinsic contribution of H₂ to promote the main reactions in DOC. It is already known that cofeeding of H₂ into the lean gas mixture may also lead to NO_x reduction to N₂O and N₂ over Pt catalysts. This process is known as H₂-SCR and has been widely investigated in the literature as reviewed by Hamada and Haneda [23].

Addition of H₂ to improve low temperature CO oxidation over Pt/Al₂O₃ catalysts as one of the main reactions in DOC has been widely studied [24-26]. It has been proposed to result from interactions between surface species causing a reduction in CO desorption activation energy [12, 27] or coupling of the CO and H₂ oxidation surface chemistries via the hydroxyl intermediate [28-30]. These mechanisms that enhance CO oxidation may also be linked to the improved NO oxidation.

As a residue that originates from unconverted fuel and lubricating oil, the presence of HC in the exhaust is common. For NO oxidation over a DOC, admission of HC such as C₃H₆ or dodecane (C₁₂H₂₆) has been found to inhibit NO oxidation and vice versa [20, 31]. Since H₂ may enhance the oxidation performance of Pt/Al₂O₃ [22], it is thus of interest to investigate the interplay between the inhibition effect of HC and promotion effect of H₂ on the NO oxidation reaction. Using Pt/Al₂O₃, addition of HC to a gas containing NO_x may also lead to its conversion to N₂O and N₂ via the HC-SCR process and addition of H₂ has also been reported to boost its low temperature activity [32].

Hydrocarbon-Selective Catalytic Reduction (HC-SCR) over silver alumina catalyst

3.1 General

Early work on NO_x removal in lean-burn or diesel engine exhaust conditions with hydrocarbon-SCR (HC-SCR) was pioneered by Iwamoto and Yahiro [33] and separate work by Held et al. [34] in the early 90s. Since then, numerous catalysts have been proposed and tested such as zeolite based catalysts, platinum group metal (PGM) catalysts and several base metal oxides [35]. It appeared eventually that the two most promising candidates for HC-SCR are Cu-ZSM5 (typical maximum activity at high temperature region around 350°C) and Pt/ Al_2O_3 (typical maximum activity at low temperature region around 250°C) [6]. However, challenges still remained since a significant amount of NO_x is emitted in a temperature window between 250 and 350°C (quite common diesel exhaust temperature) which is not effectively covered by either Pt/ Al_2O_3 or Cu-ZSM5. In addition, one shortcoming with Pt/ Al_2O_3 as a HC-SCR catalyst is its significant selectivity for production of N_2O which is one of the detrimental greenhouse gases and hence its emission to the atmosphere must be minimized.

Cu-ZSM5 as an alternative candidate for a HC-SCR catalyst unfortunately also has some limitations. It has been reported in literature that Cu-ZSM5 suffers from poor hydrothermal durability, where the activity for NO_x removal degrades in the presence of water vapor (real exhaust gas typically contains a H_2O concentration >10%) due to de-alumination of the zeolite framework at high temperature [6, 35]. Several attempts to augment the water resistance of zeolite based materials have been reported [36, 37]. However, the main issue related to poor low temperature activity over Cu-ZSM5 has hindered further development of this catalyst as a HC-SCR catalyst.

3.2 Silver alumina for HC-SCR

There is considerable interest in developing HC-SCR catalysts that are economically competitive, with a high activity over a broad temperature window, good hydrothermal stability, sulphur tolerance, as well as providing potential for a minimal fuel penalty. Silver

alumina appears to be a promising candidate for HC-SCR application and has been widely investigated since the pioneering work by Miyadera in 1993 [38]. However, it is worth mentioning that the poor performance of silver alumina catalysts in the low temperature region should have deterred much continued interest, until it was found that the addition of H₂ to the inlet feed gave a substantial increase in the low temperature activity [39, 40]. Since then, numerous studies have been devoted to investigate the role of H₂ and the reaction mechanism of H₂-assisted HC-SCR.

Silver alumina catalysts have been tested with various types of hydrocarbons (HC) i.e. short chain, long chain, aromatic, alcohol, biodiesel and real diesel fuel [41-47]. Tests with silver alumina have shown that reductants with a high carbon number were more superior than low carbon number reductants in terms of activity and tolerance to water. As the carbon number increases, the “mean bond energy” (the average of all C-H and C-C bond energies in a HC) decreases and therefore HC activation (a step in the HC-SCR process) will be accelerated [43]. However, problems related to fouling due to carbon deposition notably with long HC chains have also been reported, which decreased the HC-SCR performance [44, 48]. The use of more complex HC reductants such as aromatics gave lower activity than straight HC due to less favorable HC activation [44]. Furthermore, it has been suggested that the NO_x removal efficiency is not only influenced by the structure of HC, but also by the silver morphology over the catalyst [44].

As a result of growing interest to use bio-based fuel in the transportation sector, the feasibility to use various bio-based fuels such as alcohols (methanol and ethanol), biodiesel and DME have also been widely investigated in the literature [41, 45, 47, 49]. Since the early work on silver alumina by Miyadera [38], it has been shown that oxygenated HC (such as ethanol) is easier to be partially oxidized than non-oxygenated straight chain HC. Comparing the activity of low molecular weight alcohols, it appears that propanol and ethanol gave remarkably higher NO_x removal activity compared to methanol [43, 50]. As a result, oxygenated HC gives higher NO_x removal activity than non-oxygenated straight chain HC. Formation of gas phase H₂ or ad-H atoms from oxygenated HC has also been proposed as a reason of higher NO_x conversion with alcohols [51, 52]. Recently, it is also reported that addition of methanol instead of H₂ was found to improve octane-SCR activity over Ag/Al₂O₃ catalyst, again due to the possible formation of H₂ from methanol decomposition [53]. These results therefore show a promising application of Ag/Al₂O₃ with alcohol fuels. Commercial scale Ag based HC-SCR technology using E85 fuel as reductant has been reported by General Electric, Tenneco and Umicore to achieve as high as 85-95% NO_x conversion over a temperature range of 325-425°C [54].

The use of DME as a reductant for Ag/Al₂O₃ has also been tested. DME-SCR over Ag/Al₂O₃ showed relatively low NO_x reduction activity similar to methanol-SCR [49]. Further, Erkfeldt et al.[41] and Arve et al.[45] investigated several biodiesel fuels over silver alumina catalysts and reported considerable NO_x reduction activity at high temperature above ca. 350°C. It has been suggested that high hexadecane concentration (as a biodiesel model compound)

above 200 ppm may inhibit NO_x reduction notably at 300 and 400°C by hindering NO adsorption on the surface and difficulty to partially oxidize the adsorbed HC. While at high temperature such as 550°C, increasing HC concentration is beneficial for NO_x reduction as a result of greater oxidation of HC which appeared to facilitate HC-SCR [45].

The knowledge on the role of active sites over Ag/Al₂O₃ as a NO_x reduction catalyst is still unclear. Depending on the preparation method, several suggestions have been put forward mentioning the presence of metallic silver, oxidized silver, isolated ionic silver and silver aluminate [55, 56]. Furthermore, it has also been suggested that the role of small silver clusters (Ag_n^δ) is important [57]. Although the exact role of each possible silver site is still being investigated, it is generally accepted that metallic silver has an oxidizing function and is thus responsible for activation of HC and NO_x. Small silver clusters and oxidized silver have been proposed to activate the NO_x reduction activity by partially oxidizing the reductant and promoting surface nitrate formation. Shimizu and Satsuma have summarized various silver states as active sites in their review and references therein [43]. The proportion of small silver clusters and metallic silver depends much on the silver loading and preparation technique. With impregnation methods, high silver loading tends to produce more metallic silver while low silver loading gives a higher proportion of small clusters of silver [55]. Sol-gel methods are favorable for producing catalysts containing small silver clusters and oxidized silver which are more finely distributed in the alumina matrix [58].

3.3 Mechanistic studies of HC-SCR

One of the most challenging parts in HC-SCR over Ag/Al₂O₃ catalysts is to understand the reaction mechanism of NO_x reduction, which is particularly complicated by the nature of hydrocarbons used that contribute to the formation of a number of intermediates (both spectators and active intermediates) during reaction. Several literature reports have addressed mechanistic aspects of NO_x reduction over Ag/Al₂O₃ [35, 43, 47, 57, 60].

A general schematic diagram of the HC-SCR mechanism over Ag/Al₂O₃ is shown in Figure 3.1. Generally, the first step of HC-SCR is activation of NO and HC by O₂. NO and O₂ will form NO_x surface species (nitrates and nitrites). Strongly adsorbed nitrate is known to self-inhibit the NO_x reduction at low temperature [50, 61]. For activation of HC, the O₂ partially oxidizes the HC to form oxygenated HC surface components. Although the formation of oxygenated HC is generally agreed to occur, however, the structure and role of oxygenated HC surface compounds remains a subject of debate in the literature. Different interpretations of HC intermediates can be due to a variety of experimental conditions [43]. In the subsequent part of the HC-SCR mechanism, the nitrogen containing species are expected to react with oxygenated HC surface species forming several surface intermediates where the major surface species are R-NO (nitroso species), R-ONO (nitrite species), R-NO₂ (nitro species), R-CN (cyanide species), R-CNO (isocyanate species) and R-NH₂ (amine species) [60]. It is believed that cyanide, isocyanate and amines are the dominant routes to eventually form gaseous N₂ during the HC-SCR [62-64].

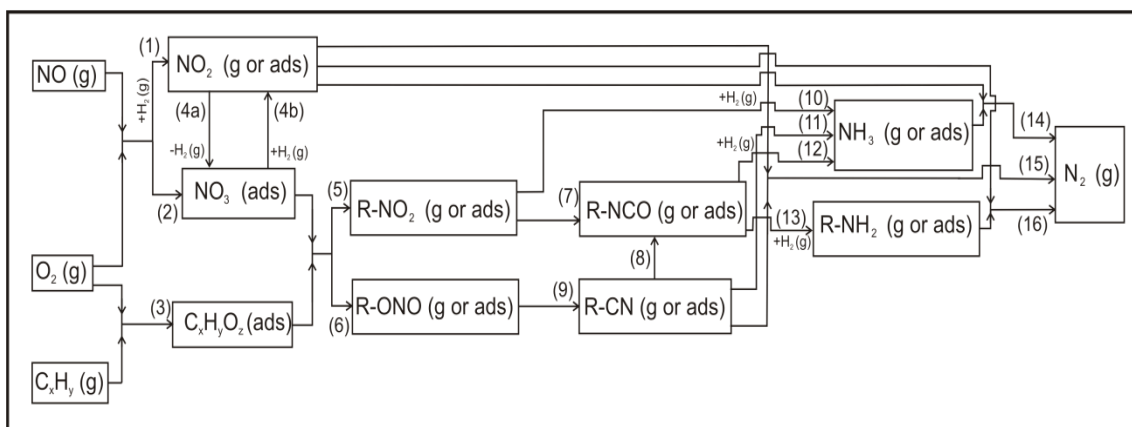


Figure 3.1 Schematic diagram of the reaction mechanism of H₂-assisted HC-SCR over Ag/Al₂O₃, adapted from [59, 60]

3.4 The effect of H₂ on HC-SCR over Ag/Al₂O₃

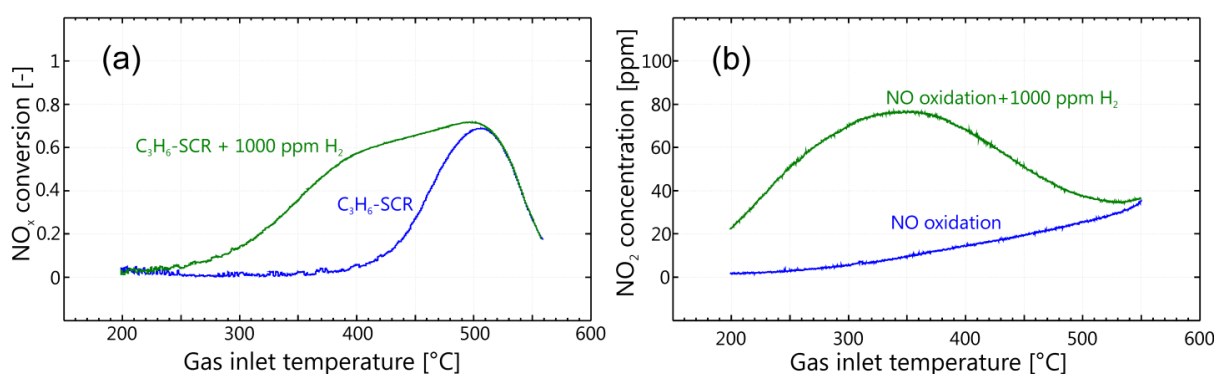


Figure 3.2 Promotional effect of H₂ to improve C₃H₆-SCR (500 ppm NO, 1000 ppm C₃H₆, 8% O₂) and NO oxidation (500 ppm NO, 8% O₂) over 2 wt.% Ag-Al₂O₃. Gas hourly space velocity (GHSV) was ca. 29000 h⁻¹.

Perhaps, the most interesting feature of the silver alumina system for HC-SCR is the fact that addition of small amounts of H₂ can strongly promote low temperature NO_x reduction activity as reported by Satokawa in the early 2000s [39, 65]. As a result, a wider temperature window for HC-SCR process is obtained as illustrated in Figure 3.2a. Another catalyst that is promoted by H₂ for HC-SCR activity is Ag-MFI [66]. Defining the exact role of H₂ in HC-SCR over Ag/Al₂O₃ is far from trivial. From literature, there are several proposed explanations for the “H₂ effect” including:

- the enhancement of the partial oxidation of the reducing agent [60, 67].
- formation of reactive N species (like –NCO species [68] or gas phase radicals [60]) from the reducing agent.
- the accelerated formation of active cationic silver clusters [43, 57].
- the destabilization of surface nitrates blocking active silver sites [40, 51, 67, 69-72]
- generation of Ag-hydride leading to formation of hydroperoxy radicals (HO₂), peroxide (O₂²⁻) and superoxide ions (O₂⁻) [57, 73].

It should also be considered that in a HC-SCR, it is possible that H₂ can have multiple roles among the effects mentioned above [40]. A study by Kim et al.[74] classified the roles of H₂ as *fast* and *slow* processes. The kinetic effect of H₂ was classified as a *fast process* in the time range of seconds. Here, H₂ activates formation of adsorbed surface species and chemical changes in oxidized silver. A morphological change such as the formation of silver clusters is classified as a *slow process* in the time scale of minutes.

It is also obvious that addition of H₂ facilitates higher NO oxidation activity over Ag/Al₂O₃ as illustrated in Figure 3.2b. Satokawa et al.[39] suggested that the increase in NO₂ yield in the presence of H₂ is due to the role of H₂ to decompose nitrate formed on Ag/Al₂O₃. Formation of nitrate itself is known to self-inhibit the NO_x reduction process over Ag/Al₂O₃ [61]. In another study, Sadokhina et al.[75] proposed that the role of H₂ in NO oxidation is indirect by promoting formation of nitrate on Ag and Al which subsequently may decompose to NO₂ in the gas phase with the aid of NO.

It is important to mention that with the addition of H₂, NH₃-SCR over Ag/Al₂O₃ was also considerably promoted [76]. For this reason, the study of Ag/Al₂O₃ for HC-SCR and NH₃-SCR has gained a lot of interest in the present literature.

3.5 Onboard H₂ production

Concentrations of H₂ in diesel exhaust gas range from very little to almost non-existent. Katare and Liang [26] reported the average molar ratio of CO/H₂ from diesel exhaust under a FTP (Federal Test Procedure) test is around 40-70 (mol/mol) with a maximum H₂ concentration of 0.07%. For gasoline exhaust, the average molar ratio of CO/H₂ is approximately 3 (mol/mol) with a maximum H₂ concentration of 2%. Therefore, other techniques, namely onboard diesel reforming, have been applied as a way to produce H₂ [77]. The produced H₂ can also be used to power a fuel cell of an APU (Auxiliary Power Unit) to support comfort systems on larger vehicles such as heavy-duty trucks and busses.

Utilization of a small amount of H₂ for the aftertreatment system will cause an increase in the fuel penalty. Kannisto et al.[78] evaluated the fuel penalty in a combined ATR (Auto Thermal Reformer) and Ag/Al₂O₃ HC-SCR system. Assuming fuel consumption and NO_x emission of 200 g/kWh and 1 g/kWh respectively, the combined use of fuel as reductant (C/N = 6-8) and for producing ca. 1000 ppm H₂ resulted in an approximately 2% fuel penalty. They also estimated that by comparing the economic price of urea, the equivalent fuel penalty for NH₃-SCR technology is approximately 0.5%. Thus, to be able to compete with existing NH₃-SCR technology, either a lower amount of H₂ for the aftertreatment process should be required and/or the efficiency of the reforming process must be higher.

Chapter 4

Experimental methods

4.1 Catalyst preparation: synthesis and washcoating

Silver alumina powder was prepared by a freeze dried sol-gel method as described by Kannisto et al. [58]. Briefly described here, aluminium isopropoxide (98+%; Aldrich) was used as a precursor of sol gel γ - Al_2O_3 . For Ag- Al_2O_3 synthesis, the solution of aluminium isopropoxide (AIP) was mixed with silver nitrate (>99.5%; VWR) in deionized water (milli-Q water). To obtain a pH of around 4.5, 10 vol.% of nitric acid solution was added gently and then the solution was stirred overnight to form a transparent aluminum hydroxide sol. Subsequently, evaporation of isopropanol was performed under reduced pressure and temperature of around 45°C. When the sol became a transparent gel, the gel was freeze dried. The resulting dry powder was then collected and crushed into a fine powder. The powder was placed in a ceramic crucible in a furnace for calcination.

Table 4-1 Summary of catalyts used in this thesis

Catalysts	Approximate Ag or Pt loading (wt.%)	Used in
Ag- Al_2O_3	2	Paper I
Al_2O_3	-	
Ag- Al_2O_3	5	Paper II
Ag- Al_2O_3	2	Paper III
Ag- Al_2O_3	2	Chapter 8
Al_2O_3	-	
Pt/ Al_2O_3	1	Paper IV

Platinum alumina powder was prepared by a wet impregnation method as described by Auvray [79]. In brief, pre-calcined γ -alumina (Puralox SBa-200, Sasol) was mixed with a certain amount of deionized “MilliQ” water under stirring and controlled pH. Nitric acid was then added drop-wise to reach a stable pH of ca. 4. A solution containing the Pt was prepared by dilution of the appropriate amount of $\text{Pt}(\text{NO}_3)_2$ (Heraeus). It was then added drop-wise to the stirred alumina slurry. During this operation, the pH decreased. The resulting solution was frozen by dipping in liquid N_2 and dried overnight under vacuum so as

to sublime the water. Eventually, the resulting catalyst powder was calcined in a furnace. Table 4-1 presents the summary of catalysts used in this thesis. Characterization of surface area and pores size distribution of powders were performed with a BET instrument (Micromeritics).

Bare cordierite monoliths (400 CPSI, 188 parallel channels with 1.1 mm open channel dimension) with 2 or 4 cm length and 2 cm diameter were used. Prior to coating, the bare monolith was calcined to remove impurities. The catalysts powder was mixed with binder boehmite (Disperal Sol P2; Condea) and then mixed with milli-Q water under vigorous stirring. The monolith was coated by either dropping it into slurry or using non-graduated pipettes to deposit the slurry uniformly onto the channels. The coated monolith was typically dried under a hot air gun at 90°C for about 5 minutes and then briefly calcined at 600°C for 1-2 minutes. The monolith was then cooled down before it was weighed. The coating process was repeated until the targeted weight of washcoat was deposited. Eventually, the coated monolith was calcined in a furnace at 550 or 600°C.

4.2 Flow reactor experiments

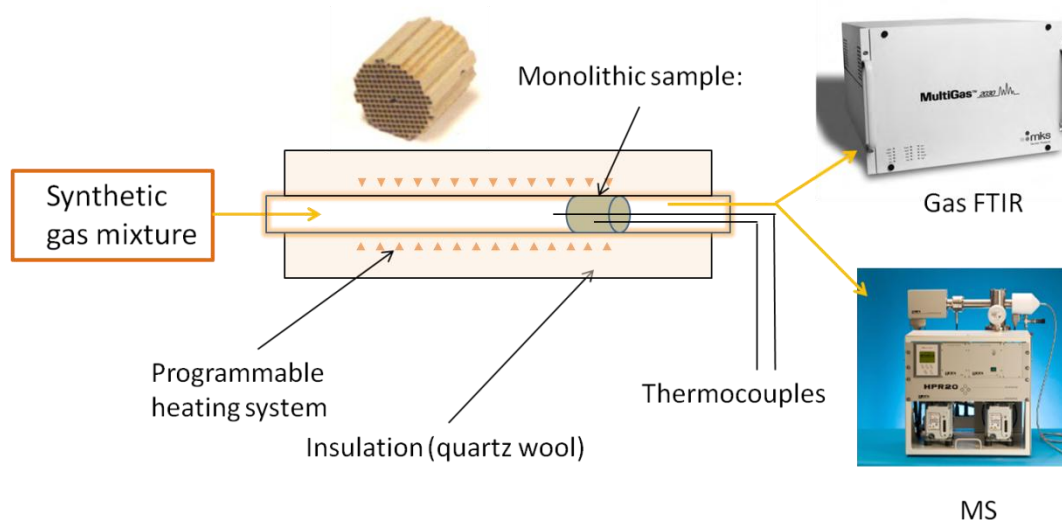


Figure 4.1 Schematic diagram of flow reactor equipment

Flow reactor experiments were used extensively as the main equipment for activity measurements. A schematic diagram of flow reactor is shown in Figure 4.1. It consists of a horizontal quartz tube (88 cm long and 2 cm diameter) heated by a helical heating coil on the outer surface of the tube. To prevent heat loss, the reactor was covered by quartz wool insulation. The monolith was placed inside the tube near to the outlet end of the tube. To avoid bypass flow around the monolith, it was sealed inside the tube by a thin layer of quartz wool. To measure and regulate temperature, two thermocouples (type K) were placed inside the sample. One was positioned at around 1 cm from the outlet end of the sample and the other one was inserted through the length of monolith until it protruded approximately 5 mm from the inlet end. The inlet temperature signal was controlled by a

Eurotherm temperature controller. The inlet gases were supplied by a number of separate mass flow controllers, whereas water vapor was provided by a controlled evaporation and mixing system (all Bronkhorst Hi-Tech). Argon was used as a carrier gas. The total typical flow of inlet gas was 3000-3500 mLn/min (1 Bar and room temperature), whereas in TPD experiments, a lower total flow was usually used.

The reactor outlet gas composition was analyzed by a MKS 2000 FTIR instrument measuring the concentrations of NO, NO₂, H₂O, N₂O and NH₃ when HC was not fed. Additional measurements from aforementioned gases were made: CO, CO₂ and C₃H₆ when C₃H₆ (propene) was added. In some cases, a small part of the outlet flow from the reactor was sampled to a Hiden HPR 20 quadrupole mass spectrometer (MS) for gas analysis especially for diatomic gas measurements such as H₂, N₂, and O₂.

4.3 In-situ DRIFT spectroscopy

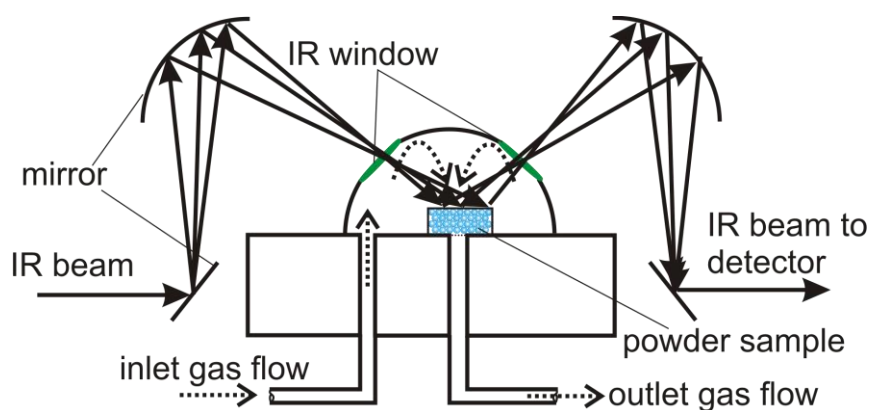


Figure 4.2 Schematic diagram of DRIFT Spectroscopy

Diffuse Reflectance Infrared Fourier Transform Spectroscopy (DRIFTS) is a useful in-situ technique to identify adsorbed surface species on a catalyst surface by detecting molecular vibration using mid-region infrared energy (wavenumber 200-4000 cm⁻¹) [80]. In DRIFT spectroscopy, an infrared (IR) source irradiates an IR beam which is reflected to enter the interior structure of a powder sample. The unabsorbed IR beam is transmitted to other particles or reflected out to a collecting mirror and sent to an IR beam detector for further analysis. A schematic diagram of DRIFT spectroscopy is depicted in Figure 4.2. The energy difference in vibrational states will characterize specific types of surface species. Adsorbed surface species on a catalyst will partially absorb IR photons and cause vibrations. However, only vibrations that trigger dipole moment changes can be detected with this technique [80]. The change of the dipole moment is proportional to the intensity of the IR band.

The DRIFT instrument used in this work was a Bio Rad FTS6000 spectrometer. One of the advantages of using DRIFT is the relatively simple operating procedure, where the analyzed sample can be mounted directly onto a DRIFT instrument for analysis. The powder sample was placed in a sample holder (supported by a metallic grid) of a high temperature Harrick Praying Mantis cell coated with Silcolloy® 1000 and equipped with a KBr window. To

regulate temperature, the DRIFT cell was equipped with a Eurotherm heating system and water cooling system. In addition, a K-type thermocouple was placed near the sample holder to indicate the bed temperature. The gases were supplied by a number of mass flow controllers (Bronkhorst Hi-Tech). A fast switching valve is installed in the feed gas lines to allow a smooth step response during experiments. The outlet gas from the DRIFT instrument is continuously sampled by a mass spectrometer (Balzer Quadstar 420) to facilitate gas analysis.

Chapter 5

Modeling methods

5.1 General

The role of a kinetic model is to consolidate available experimental data with theoretical principles. It is hoped that a realistic kinetic model can capture the physical and chemical phenomena on the catalyst and hence it can give essential insights in the development of a catalyst. In a modern catalysis research cycle, development of a catalyst is not merely attributed to the knowledge of catalyst synthesis and surface science, but also uses kinetic modeling to elucidate the important steps in a reaction network (Figure 5.1). There are three interconnected aspects i.e. synthesis, performance and design that are all important to create a successful catalyst for industrial applications. A better understanding of kinetic information will improve the synthesis and design aspects of the catalyst to obtain the best performance of a catalyst [81].

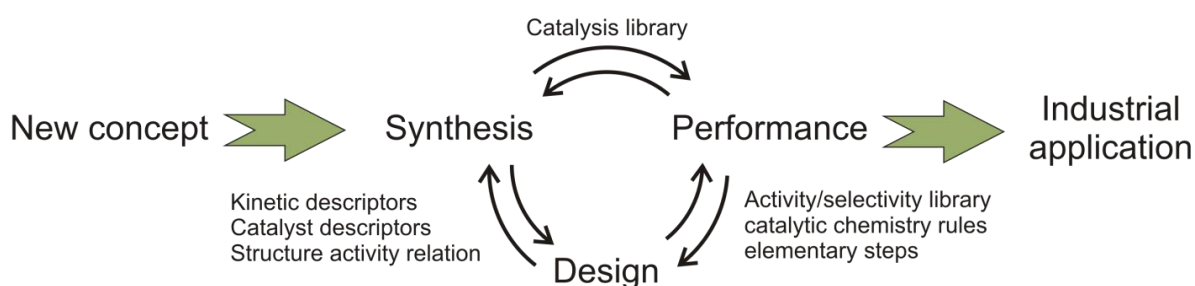


Figure 5.1 Schematic diagram of modern catalysis development. Adapted from [81]

5.2 Kinetic modeling: global and microkinetic approaches

In this work, both global and microkinetic modeling approaches were used. A global kinetic model combines adsorption, surface reaction and desorption steps with a global rate expression. Alternatively, one way to resolve the kinetic rate expression is by assuming that one of the steps (can be adsorption, surface reaction or desorption) is the rate determining step and all remaining steps in quasi-equilibrium. Generally, kinetic rate expressions of global kinetic models can then be written as a function of gas phase properties as shown in equation (5.1) [81].

$$r = (\text{kinetic factor}) \cdot \frac{(\text{driving - force group})}{(\text{adsorption group})} \quad (5.1)$$

A microkinetic analysis is a tool to investigate the reaction mechanism over heterogeneous catalysis by assembling several elementary steps without pre-assuming that any step is the rate determining step or intermediate surface species most abundant [82]. Microkinetic analysis will typically generate a large number of elementary steps and form a highly correlated and non-linear mathematical system. Since a wide range of kinetic parameter values may fit the experimental data, determination of kinetic parameters should be partially based on theoretical principles (physically and chemically sound) and other correlations to describe the experimental data with the proposed microkinetic model.

A mean-field approximation is often used along with a microkinetic analysis which assumes [83, 84]:

- random distribution of all adsorbed species over the catalyst surface.
- the absence of interactions among the adsorbed species.

With these assumptions, the probability for all active sites (i.e. neglecting differences between step and terrace sites) to adsorb gas phase reactants is considered equal. Microkinetic and global kinetic modeling along with mean-field approximation has been used in **paper II and III**. A more detailed work accounting for interaction of surface species on steps and terraces of active sites is typically conducted by using kinetic Monte Carlo simulations. An example of comprehensive overview of this technique has been presented by Reuter [85].

In a microkinetic model, all elementary steps are described as reversible reactions and the rate of an elementary step as either a forward or backward reaction can be expressed as:

$$r_j = k_j \cdot \prod_{i=1}^{i=I} y_i^{\nu_i} \cdot \prod_{w=1}^{w=W} \theta_w^{\nu_w} \quad (5.2)$$

$$k_j = A_{ij} \cdot \exp\left(\frac{-E_{a_j}}{R \cdot T}\right) \quad (5.3)$$

From equation (5.2), it can be noted that the order of the reaction with respect to gas phase or surface species concentration (ν) corresponds to the stoichiometric coefficient of the reactant. Preexponential factors and activation energies are the common kinetic parameters to estimate as described in the famous Arrhenius equation (5.3). In order to obtain reasonable kinetic parameter values, there are several strategies to determine kinetic parameters [8]:

- investigating a sub-system from a larger system and determine the kinetic parameters independently
- information from literature
- thermodynamic restrictions

- collision theory and transition state theory
- statistical thermodynamics
- regression analysis with experimental data.

A combination of these methods can be used to obtain kinetic information from parameter estimation.

Estimation of preexponential factors for adsorption steps is generally taken from collision theory or transition state theory. The sticking coefficient at zero coverage for collision theory is then fixed or estimated from literature values. For desorption and surface reaction steps, a reasonable limit for preexponential factors can be obtained from transition state theory [82].

Estimation of activation energies can be approximated from DFT calculations, bond-order conservation theory (BOC) or via the related but more advanced UBI-QEP (Unity Bond Index-Quadratic Exponential Potential) calculations and literature values [82]. To illustrate, literature values of UBI-QEP estimates have been used in **paper II** to estimate activation energies of desorption steps [86].

Thermodynamic restrictions based on overall gas phase reactions can also be applied in microkinetic modeling. Thermodynamic restrictions for all elementary steps can be shown as:

$$\prod_i \left(\frac{A_{i_f}}{A_{i_b}}\right)^{\nu_i} = \exp\left(\frac{\Delta S_R}{R}\right) \quad (5.4)$$

$$\Delta H_R = \sum_i \nu_i \cdot E_{a_f} - \sum_i \nu_i \cdot E_{a_b} \quad (5.5)$$

5.3 Reactor model

Monolith-supported catalysts are the standard form of catalysts used in this thesis. For modeling purposes, the monolith catalyst or monolith reactor was simulated with a single channel reactor model as depicted in Figure 5.2. Here, the reactor model only briefly presented. A more detailed description of reactor model including mass and heat transport equations used in the model can be found in **Paper II** page 385 to 386.

As seen in Figure 5.2a, the monolith reactor was modeled as tanks-in-series where the channel was segmented both in the axial and radial directions. By dividing the washcoat into several layers (Figure 5.2b), the reactor model is able to account for internal mass transfer resistance which is commonly excluded in a conventional kinetic model. In each tank and layer, mass and heat balance equations were solved for all gas and adsorbed surface species. The theoretical number of tanks required in the axial direction can be estimated using the dispersion model for laminar flow in an open-open system as described in [87].

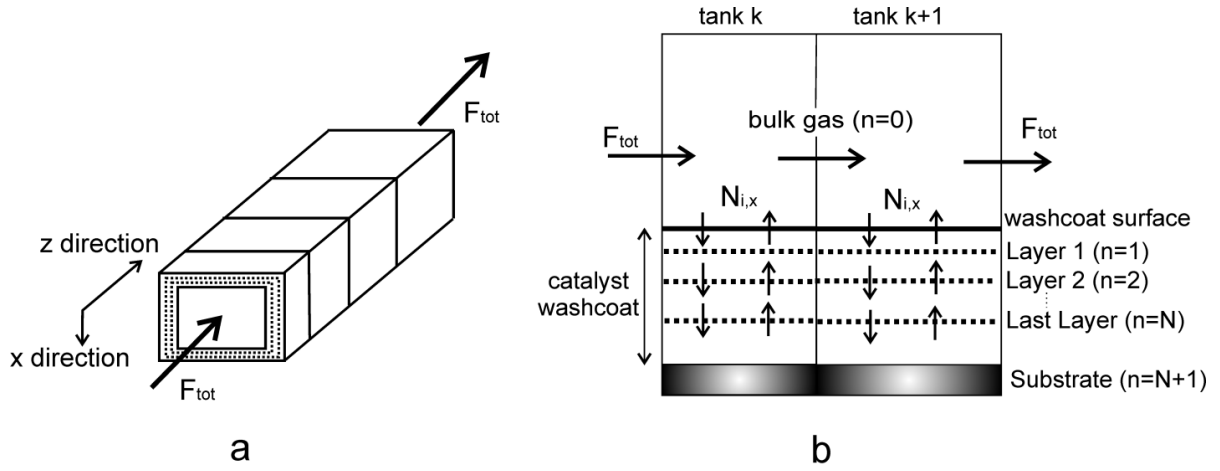


Figure 5.2 Single channel monolith model showing the washcoat discretization in axial (a) and radial direction (b) with arrows indicating mass transport.

The theoretical number of tanks-in-series (n) typically gives a large number of tanks and hence requires extensive computational time. Therefore, an alternative approach to estimate the number of tanks-in-series was employed by investigating the effect of varying the number of tanks and layers on the calculated sum of the squares of error (SSE). It is also important to mention that the size of each tank (in axial direction) and layer (in radial direction) was gradually varied as illustrated in Figure 5.2 to obtain a finer discretization where the concentration gradients were steeper.

5.4 Modeling of mass balance

The gas phase mass balance in each tank was modeled as a steady state mass balance between axial convective flow and radial mass transfer as shown in equation 5.6.

$$F_{tot} \cdot (y_{i,k-1,0} - y_{i,k,0}) - \Gamma_{i,k,0} \cdot (C_{i,k,0} - C_{i,k,1}) = 0 \quad (5.6)$$

A film model was applied to describe the mass and heat transport from the bulk gas to the washcoat. The values of transport coefficients varied along the axial direction of the channel according to the empirical correlation given by Hawthorne [88].

The mass balance inside the washcoat is developed for each layer and characterized by radial diffusion (perpendicular to the bulk flow) and reactions. Equation 5.7 shows the mass balance in each layer (for layers $n \geq 1$).

$$\Gamma_{i,k,n-1} \cdot (C_{i,k,n-1} - C_{i,k,n}) - \Gamma_{i,k,n} \cdot (C_{i,k,n} - C_{i,k,n+1}) + \sum_j \nu_{i,j} \cdot r_{j,k,n} \cdot w_{s,k,n} = 0 \quad (5.7)$$

While the overall mass transport coefficient (Γ) between gas phase-washcoat and between each layer in washcoat can be written as:

$$\Gamma_{i,k,0} = \frac{A_k}{\frac{1}{kc_{i,k}} + \frac{0.5 \cdot \Delta X_1}{D_{eff,i,k}}} \quad \text{and} \quad \Gamma_{i,k,n} = \frac{A_k}{\frac{0.5 \cdot \Delta X_n}{D_{eff,i,k}} + \frac{0.5 \cdot \Delta X_{n+1}}{D_{eff,i,k}}} \quad (5.8)$$

However for the bottom layer ($n = N$), $\Gamma_{i,k,N} = 0$, inferring no transport to the monolith substrate.

The effective washcoat diffusivity was calculated from the Bosanquet [89] correlation by including gas diffusivity, Knudsen diffusivity and a factor accounting for the porosity and tortuosity of the washcoat. Gas diffusivity was calculated from the Fuller-Schettlet-Gidding relationship [90] and corrected for the current segmental washcoat temperature while Knudsen diffusivity was approximated by using the semi-empirical Knudsen correlation [91].

A microkinetic model in this work was used to describe the transient simulations and therefore should be able to explain the dynamic change of surface species coverages. The dynamic mass balance of surface species is dictated by their involvement in reactions and expressed as:

$$N_c \cdot \frac{d\theta_{w,k,n}}{dt} = \sum_j r_{j,k,n} \cdot \chi_{w,j} \quad (5.9)$$

5.5 Modeling of heat balance

The reactor model used here also facilitates heat balance calculations. The gas phase heat balance in each tank is assumed to be steady-state and adiabatic :

$$F_{tot} \cdot c p_g \cdot (T_{g,k-1} - T_{g,k}) - h_k \cdot A_k \cdot (T_{g,k} - T_{s,k}) = 0 \quad (5.10)$$

Accumulation terms in the gas phase mass balances (equations 5.6) and the gas phase heat balance (equation 5.10) were neglected because the characteristic time constants for these transport processes is considerably smaller compared to accumulation of surface species (equation 5.9) and heat in the solids (catalyst and washcoat).

For the heat balance in the washcoat, heat transfer in the radial direction within the washcoat was neglected. However, heat accumulation and transport between solid (washcoat and substrate) and gas in each tank was included. Also, axial heat conduction between solid segments and heat contribution from reactions in each tank were included.

5.6 Matlab implementation: simulation and parameter estimation

The mass and energy balances were expanded for each gas phase component, surface component, tank and layer. The solution of these equations gives the concentrations of gas and surface components, gas and catalyst temperature in each layer and tank for each measurement time. The resulting differential and algebraic (DAE) equations were solved using the ODE15s function in Matlab R2008a[®] and the results were stored in a large multi-dimensional matrix.

Parameter fitting was performed using the lsqnonlin function in Matlab R2008a[®]. This function uses a gradient search method to perform non-linear regression. For modeling purposes, the rate constant which follows the Arrhenius expression (equation 5.3) needed to be modified to decouple the high correlation between preexponential factors and activation energies. As a result, the fitted parameters were logarithmic values of the rate

constant ($\ln(k_{ref})$) at the average experimental temperature (T_{ref}) and the activation energy (Ea) as shown as:

$$k_j = \exp\left(\ln(k_{ref})_j - \frac{Ea_j}{R}\left(\frac{1}{T_{s,k}} - \frac{1}{T_{ref}}\right)\right) \quad (5.11)$$

Prior to the fitting, each parameter was scaled according to:

$$\beta_{scaled} = \frac{\beta_{unscaled} - \beta_{initial\ value}}{range} \quad (5.12)$$

The scaling factor called *range* was set so that a scaled parameter value of +1 approximately doubled the reaction rate from the initial parameter value and a scaled value of -1 corresponded to approximately half the reaction rate. Subsequently, the upper and lower bounds were determined in accordance with the scaled values. The objective of non-linear regression was to minimize the sum of the square of error (SSE) where the residuals were typically calculated from outlet gas measured and calculated mole fractions.

Chapter 6

Stability of surface NO_x species: TPD and DRIFTS studies

6.1 Roles of surface NO_x species

As seen from the proposed HC-SCR mechanism in Figure 3.1, activation of NO_x is characterized by formation of surface NO_x species mainly as nitrate and/or nitrite species. Subsequently, surface NO_x species play a role by reacting with oxygenated HC (a result of HC activation) to form a number of intermediates which eventually lead to the formation of N₂. For this reason, surface NO_x species have been suggested to be important intermediates and therefore it is important to understand their formation, stability and reactivity to elucidate the mechanism of HC-SCR.

It is interesting to note that H₂ may play a dual role in its interaction with nitrate species. On one hand, H₂ has been proposed to promote elimination of nitrates during H₂-assisted HC-SCR [59, 67, 70, 92]. On the other hand, it has also been shown from FTIR studies that H₂ activates accumulation of nitrates on the surface during NO oxidation [56, 67, 73, 93]. Thus, an additional objective for studying surface NO_x species was to examine whether these seemingly contradictory roles for H₂ could be compatible.

In order to investigate and clarify the characteristics and stability of nitrate species on Ag-Al₂O₃, a series of in-situ DRIFTS and TPD studies have been conducted. Here, the focus has been placed on understanding the role of H₂ to modify the surface NO_x species in relation to the promotional effect of H₂ for NO oxidation and C₃H₆-SCR. A more detail description of these studies can be found in **Paper I**.

6.2 TPD studies of NO_x

Temperature-programmed desorption (TPD) is a useful technique to investigate the thermal stability of adsorbed species. TPD studies to investigate the stability of surface NO_x species over Ag/Al₂O₃ have been reported in the literature [50, 75, 94, 95]. Figure 6.1 shows desorption profiles from TPD of NO_x.

As seen from the upper panel of Figure 6.1 for TPD following an NO oxidation pretreatment, two desorption peaks were observed: a low temperature (LT) peak at 277-340°C and a high temperature (HT) peak at ca. 440°C. It is noteworthy that the LT peaks were skewed to higher temperatures with increasing adsorption temperature. The major NO_x components desorbed were NO at both LT and HT peaks whereas NO₂ was only observed at the LT peak following adsorption at 200 and 250°C.

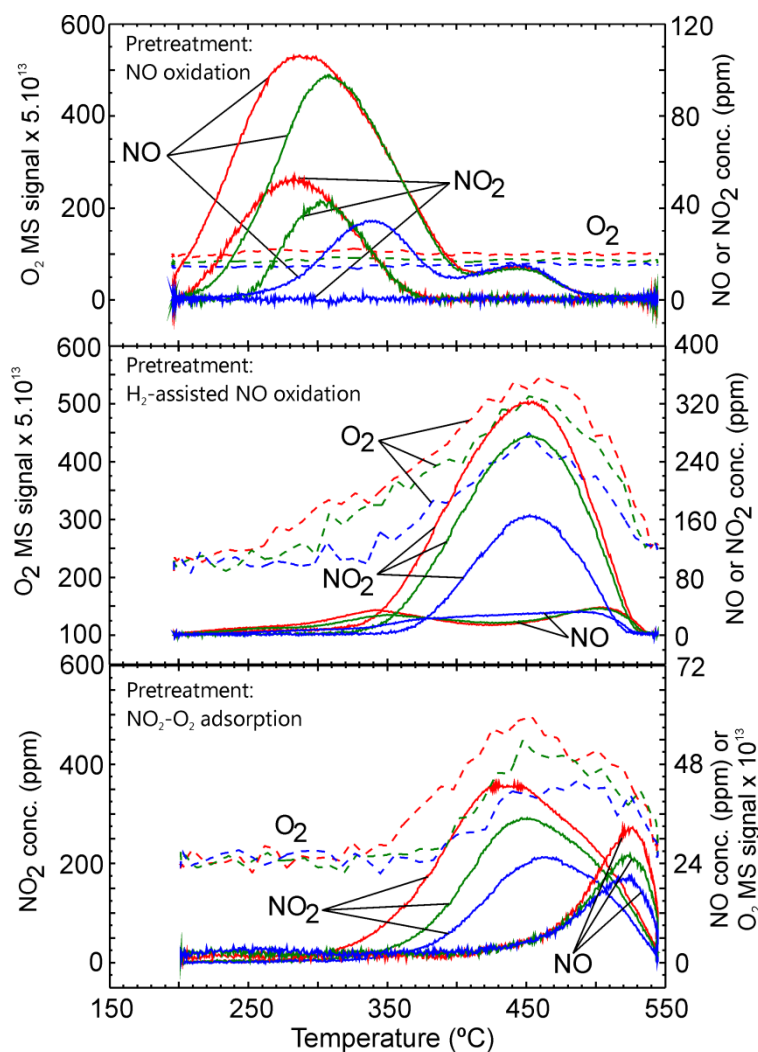


Figure 6.1 Desorption profiles of TPD NO_x in Ar flow over 2 wt.% Ag-Al₂O₃ catalyst following adsorption treatments at 200 (red), 250 (green) and 300°C (blue). Preceding adsorption condition from upper panel to lower panel respectively: 500 ppm NO + 4% O₂ (total flow of 1500 ml/min.), 500 ppm NO + 4% O₂ + 0.1% H₂ (total flow of 1500 ml/min.) and 150 ppm NO₂ + 4% O₂ (total flow of 3500 ml/min.)

Interestingly, desorption of the LT peak was not accompanied by O₂ desorption. DRIFT analysis (discussed below in section 6.3 as well as in **Paper I**) indicated that nitrates were a key surface species that is also related to the LT peak. Hence, this indicates that adsorption of NO and NO₂ over oxidized silver yielded formation of nitrate species by borrowing O atoms from oxidized Ag [96] or Al₂O₃ [97]. Decomposition of the LT surface NO_x species apparently left borrowed O atoms on Ag and Al₂O₃.

As illustrated previously in Figure 3.2b, addition of H₂ clearly promoted NO oxidation reaction over Ag/Al₂O₃. From TPD results following pretreatment in H₂-assisted NO oxidation (middle panel of Figure 6.1), it can be noted that along with higher activity for NO oxidation in the presence of H₂, the LT peak observed from NO-O₂ TPD was significantly suppressed and shifted towards the HT peak. The shift was also accompanied by higher total quantities of NO_x adsorbed and desorbed. H₂ induced NO_x adsorption over Ag-Al₂O₃ can then be related to the increase of the HT surface NO_x species. Due to the fact that the LT peak decomposed thermally at higher adsorption temperatures and was suppressed significantly in presence of H₂ which both gave higher NO oxidation conversion, it is therefore reasonable to assign the LT peak as the result of the decomposition of nitrates on the active sites.

The lower panel of Figure 6.1 shows the desorption profile following pretreatment with NO₂-O₂ adsorption. As displayed here, a substantial release of NO₂ was also observed that peaked at 440-460°C similar to the desorption profile following H₂-assisted NO oxidation (middle panel of Figure 6.1). Further, additional experiments for NO₂-O₂ TPD on Al₂O₃ (not shown here) gave a similar TPD profile as in Ag-Al₂O₃. Therefore, it was evident that the HT nitrate results from NO₂ adsorption and primarily located on the Al₂O₃ support. It is also then likely that the HT nitrates formed on the Al₂O₃ support are spectator surface species. From literature, a reaction path of NO_x storage by a spillover mechanism has been proposed [70, 75, 98]. An alternative mechanism of NO_x storage by NO₂ readsorption on the Al₂O₃ support has also been proposed [51]. Based on the results of these TPD studies, it is indicative that the NO₂ readsorption mechanism is most probable for NO_x storage on Al₂O₃ as it is related to gas phase NO₂. However, this does not negate the possibility that a spillover mechanism also contributes to NO_x storage on Ag-Al₂O₃.

Quantitative analysis was performed by integrating the amount of LT NO_x species from Ag-Al₂O₃ and Al₂O₃ to identify the amount of surface NO_x species possibly on active sites (Figure 6.2a). At 300°C, it could be observed that the amount of surface NO_x species on Ag-Al₂O₃ was more or less equal to Al₂O₃, thereby indicating that Ag sites were largely free from LT surface NO_x species by this temperature. Figure 6.2b compares the calculated reaction rates for NO oxidation and H₂-assisted NO oxidation during adsorption steps. As seen here, the rate of NO₂ formation was always higher in the presence of H₂ at all temperatures, even at 300°C where Ag was largely free from the presumably inhibiting LT NO_x species. If removal of inhibiting nitrate species was the only promoting role of H₂ for NO oxidation, one would expect the NO oxidation reaction rates with and without H₂ feed to be nearly equal at 300°C. If all inhibiting surface NO_x species were thermally removed at 300°C, comparison of reaction rates at this temperature indicates that as much as 60% of total rate with H₂ feed could not be due to removal of inhibiting surface NO_x. Therefore, these findings indicate that H₂ should have additional promoting roles.

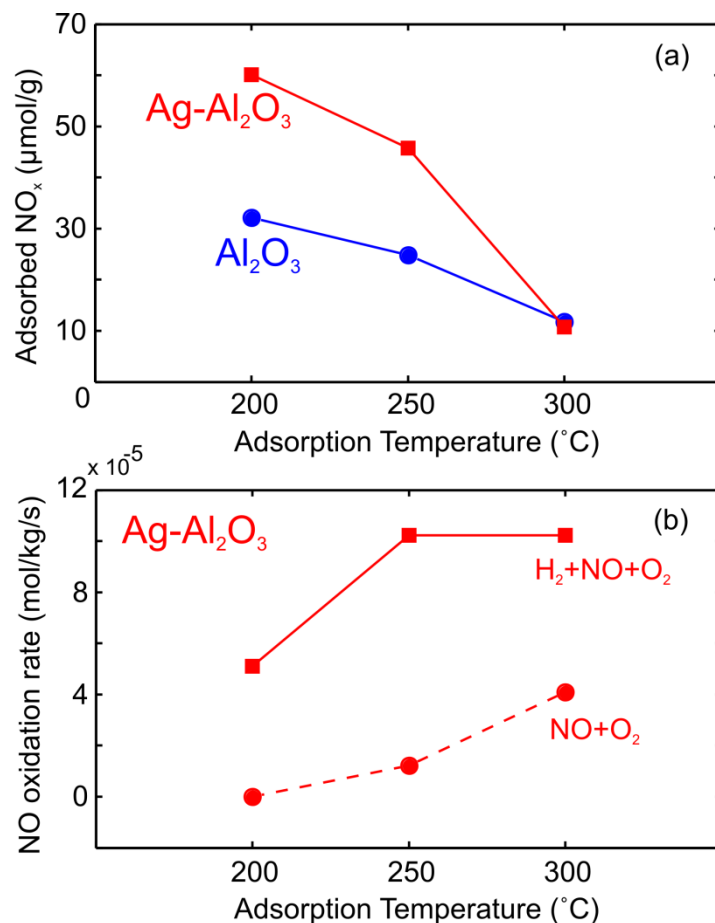


Figure 6.2 The amount of surface NO_x species from integration of LT desorption peak after NO-O_2 adsorption over $\text{Ag-Al}_2\text{O}_3$ and Al_2O_3 (upper panel, a) and reaction rate for NO oxidation and H_2 -assisted NO oxidation over $\text{Ag-Al}_2\text{O}_3$ (lower panel, b)

6.3 Stability of surface NO_x species from in-situ DRIFT Spectroscopy

Figure 6.3 shows the ensuing evolution of IR spectra as a result of an increase in cell temperature after adsorption of NO_x . Peak assignments were mainly taken from [98, 99] where the presence of monodentate, bidentate and bridging nitrates is observable. From DRIFT results, the thermal stability of nitrate species were found to be in the order of bridging < bidentate < monodentate nitrate and therefore it is reasonable to regard the LT desorption peak to primarily originate from the decomposition of bidentate and bridging nitrate species as in agreement with [50].

In the presence of H_2 in the feed, it is apparent that the formation of the bidentate nitrate at 1248 cm^{-1} was less pronounced. It is therefore suggested that the vibration of bidentate nitrate at 1248 cm^{-1} can also be associated with the LT desorption peak. By associating TPD and DRIFT, it is suggested that H_2 eliminated surface nitrate species on active sites (LT peak) which is predominantly as bidentate nitrate (1248 cm^{-1}).

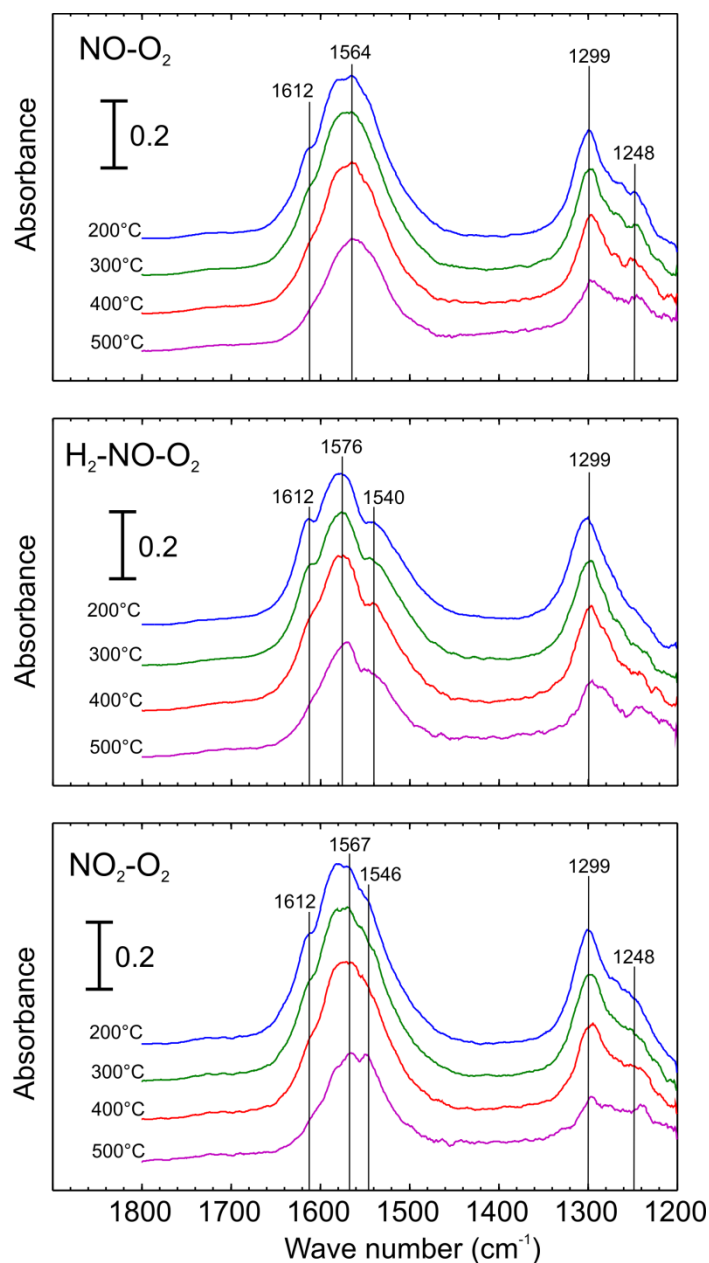


Figure 6.3 DRIFT Spectra of adsorbed species during temperature ramp following adsorption of NO oxidation (top), H₂-assisted NO oxidation (centre) and NO₂-O₂ adsorption (bottom) over 2 wt.% Ag-Al₂O₃ at 200°C. Adsorption conditions from upper to lower panel, respectively: 1000 ppm NO + 8% O₂, 1000 ppm NO + 8% O₂ + 0.1% H₂ and 300 ppm NO₂ + 8% O₂

6.4 Mechanistic insight regarding C₃H₆-SCR and H₂-assisted C₃H₆-SCR

A series of TPD studies were also conducted to investigate the quantities and nature of adsorbed NO_x and CO_x species during C₃H₆-SCR and H₂-assisted C₃H₆-SCR over the Ag-Al₂O₃ catalyst. Figure 6.4 presents the NO_x and CO_x desorption profiles following adsorption conditions of C₃H₆-SCR and H₂-assisted C₃H₆-SCR.

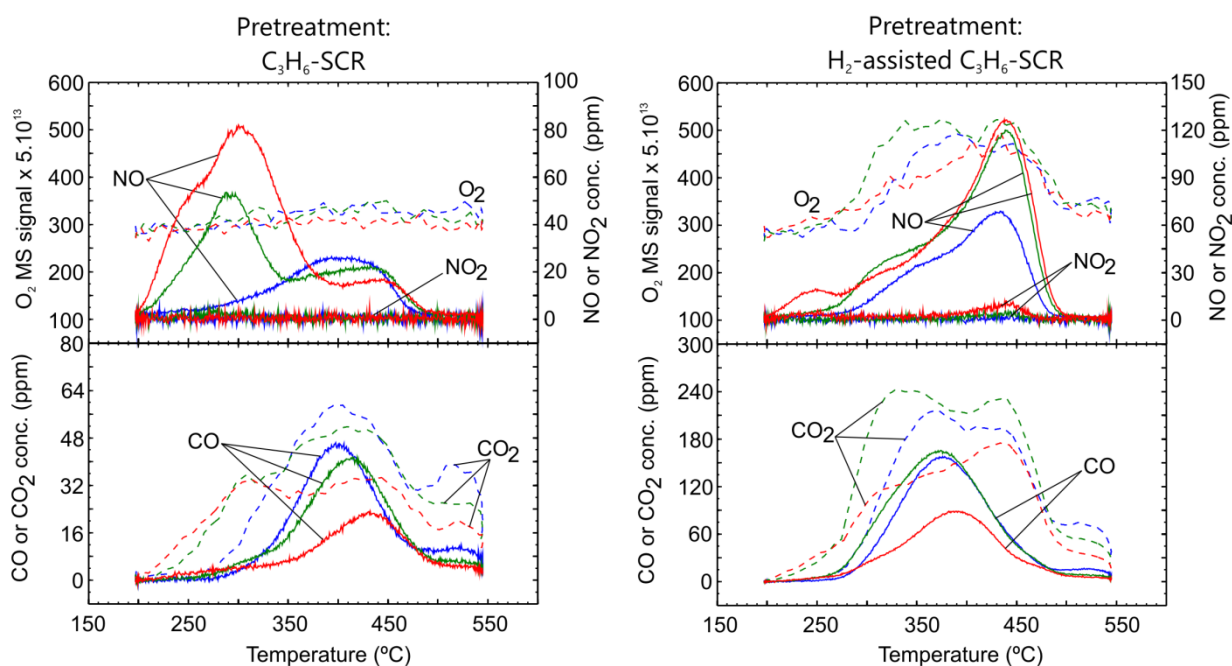


Figure 6.4 Desorption profiles following C_3H_6 -SCR and H_2 -assisted C_3H_6 -SCR in Ar flow over 2 wt. % Ag- Al_2O_3 at 200 (red), 250 (green) and 300°C (blue). Preceding adsorption conditions: 500 ppm NO + 4% O_2 + 0.1% C_3H_6 with 0 or 0.1% H_2 (total flow of 1500 ml/min).

As seen in Figure 6.4, two remarkable NO_x peaks attributable to LT and HT peak were observed following C_3H_6 -SCR. By comparing the NO_x desorption profile for C_3H_6 -SCR (Figure 6.4) and NO oxidation (Figure 6.1), both of them have a similar profile with LT and HT NO_x desorption peaks. This presence of both LT and HT nitrates in approximately the same temperature range indicates that NO oxidation and C_3H_6 -SCR share some mechanistic features.

The improvement in NO_x reduction activity for H_2 -assisted C_3H_6 -SCR (Figure 6.4) was accompanied by a significant decrease in the LT NO_x desorption peak. At the same time, the HT NO_x desorption peak increased remarkably. Therefore, again removal of the inhibiting LT nitrate, in this case aided by reaction with H_2 , improved the NO_x reduction activity. The HT peak mostly consists of NO probably because the catalyst also contained adsorbed HC which was oxidized by the adsorbed NO_x species during their decomposition and desorption. It can also be seen that the HT nitrate peak had a broad shoulder towards lower temperatures. This shoulder probably results from the presence of the adsorbed HC species acting as reductants and destabilizing the nitrate species to cause some lower temperature NO_x decomposition.

From the desorption profiles of CO and CO_2 for H_2 -assisted C_3H_6 -SCR, one can observe that a CO peak was obtained at lower temperature compared to the one in the absence of H_2 . Furthermore, the concentration of CO_x released was much higher than in the absence of H_2 , consistent with the higher conversion of C_3H_6 obtained with addition of H_2 . Higher concentrations of desorbed CO and CO_2 infer that H_2 has a promotional effect on low temperature C_3H_6 activation. HC activation to form oxidized HC species, itself is often

suggested as a key step in HC-SCR over Ag-Al₂O₃ [40, 67, 92]. This greater formation of surface HC and oxidized HC in the presence of H₂ is likely linked to the removal of inhibiting nitrate species as suggested by the suppression of the LT nitrates also with H₂. There was also a broadening and shift to lower temperature of the CO_x desorption peaks with the addition of H₂ which suggests that a greater quantity of possibly more reactive adsorbed HC species with lower thermal stabilities were formed. This perhaps points to the fact that H₂ may have other effects to promote the NO_x reduction activity in addition to removal of inhibiting nitrate species.

Greater accumulation of adsorbed CO_x due to both C₃H₆-SCR and H₂-assisted C₃H₆-SCR pretreatments at elevated temperatures indicates that the reactions to activate the HC and form oxygenated HC on the surface have relatively high activation energies. In other words, the activation energy to partially oxidize HC to form oxygenated HC species is higher than the activation energy of subsequent reactions between surface NO_x species with oxygenated HC species that lead to formation of N₂. Greater accumulation of oxygenated HC surface species may also be due to less inhibiting nitrates covering the active sites where oxygenated HC are formed.

In this series of studies, it seems that the promoting role of H₂ appears to be only partially due to the removal of inhibiting surface NO_x species. As a result the findings here support the possibility of other H₂ promoting roles as already described in the literature [39, 40, 59, 67, 92]. It has however been observed here that the formation of surface nitrate species in the absence of H₂ depends on the donation of oxygen from surface oxides. As a result the removal or prevented formation of these nitrate species caused by H₂ may be linked to some partial reduction of Ag species and thus formation of sites with enhanced activity.

Kinetic studies of the H₂ effect on NO oxidation and C₃H₆-SCR over Ag-Al₂O₃

7.1 General

One approach to investigate a large and complex reaction mechanism as exemplified by HC-SCR over Ag/Al₂O₃ catalyst is to divide it into simpler subsystems. As a part of the HC-SCR reaction mechanism, NO oxidation to NO₂ has been investigated as an important sub-reaction within HC-SCR [56, 93, 100]. As shown in Figure 3.2b, Ag-Al₂O₃ is considered as a poor catalyst for NO oxidation [56, 101], however the addition of H₂ dramatically improves its low temperature activity even with the presence or absence of H₂O in the feed [39, 56, 73, 92, 102]. TPD results shown previously in Chapter 6 show that there are common features of adsorbed NO_x species between NO oxidation and C₃H₆-SCR. Therefore, it is also probable that the mechanism by which H₂ promotes low temperature NO oxidation shares some common features with how H₂ promotes low temperature HC-SCR over Ag-Al₂O₃.

For mechanistic studies, kinetic models of H₂ effect have been constructed with the following featured highlights:

- In **paper II**, a microkinetic model for H₂-assisted NO oxidation was examined. Here, the single role of H₂ to remove self-inhibiting nitrate was proposed.
- In **paper III**, a global kinetic model to describe the promoting effect of H₂ on NO oxidation and C₃H₆-SCR was proposed. A wide range of feed and reaction conditions were examined. Here, the proposed role of H₂ was expanded not only to remove inhibiting nitrate but also to form new active sites.

7.2 Microkinetic modeling of H₂-assisted NO oxidation (Paper II)

The kinetic behavior of NO oxidation over silver alumina was investigated using transient data generated by a reduced factorial Design of Experiments (DOE). DOE has been found to be a useful method to investigate the influence of several controllable factors on some measurable effects. Here, the feed concentrations and feed temperature were varied systematically between low and high levels around a centre point condition. The experiments were performed in three batches with constant temperatures and transient

switches in the feed concentrations of reactants. Table 7-1 shows the levels of concentrations and temperature used to study the kinetic behavior of NO oxidation.

Table 7-1 The concentration and temperature levels in DOE of NO oxidation

	NO (ppm)	O ₂ (%)	NO ₂ (ppm)	H ₂ (%)	T (°C)
low (-1)	400	6	0	0	250
centre (0)	600	7	50	0.1	325
high (+1)	800	8	100	0.2	400

The effect of varied factors

The steady-state results from the reduced factorial design of experiments were analyzed by multi-linear regression (MLR) analysis. The MLR model gave a coefficient of determination of 0.994 and the normalized coefficient plot including their 95% confidence intervals are shown in Figure 7.1.

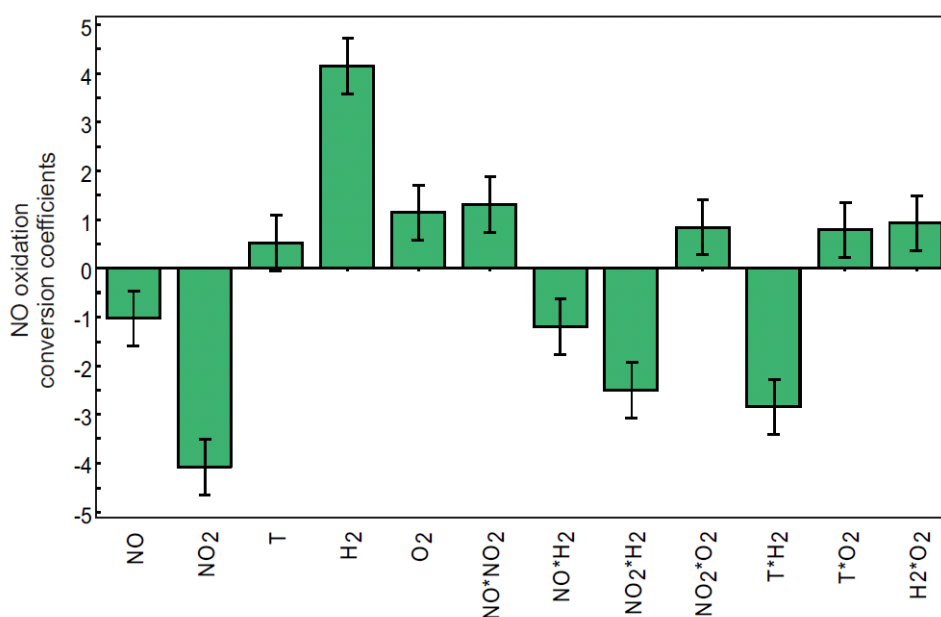


Figure 7.1 Normalized coefficient plots from MLR with 95% confidence interval bars

The magnitude and trend of the coefficients were proportional to their effect on NO oxidation conversion. The results from MLR analysis was used to support the development of the reaction mechanism in the microkinetic model. Some important aspects from MLR analysis can briefly be summarized as follow:

- H₂ clearly promoted the NO oxidation conversion as illustrated by its positive coefficient.
- The individual effects of NO and NO₂ were both negative on NO oxidation conversion. This can be rationalized by formation of self-inhibiting surface nitrates from NO and NO₂, since both are precursors to surface nitrates in the absence of HC.

Kinetic analysis

A Langmuir–Hinshelwood based reaction mechanism was used to model the oxidation of NO and H₂ involving 5 gas phase species: NO, O₂, NO₂, H₂ and H₂O. In addition, 6 surface components (NO*, O*, NO₂*, NO₃*, H* and OH*) were considered as well as vacant sites (*). Molecular adsorption was used to characterize the adsorption of NO and NO₂, whereas dissociative adsorption was used for O₂, H₂ and H₂O [103, 104]. There were 4 reversible surface reactions in the reaction network which explained the formation or consumption of NO₂*, the inhibition effect by NO₃* and the effect of H*. In total there were 18 elementary steps used in the microkinetic model. It is important to mention that the reaction mechanism was also developed based on multi-linear regression analysis using the steady state results from DOE experiments. Figure 7.2 shows all elementary steps used in the model as well as highlighting the role of H₂.

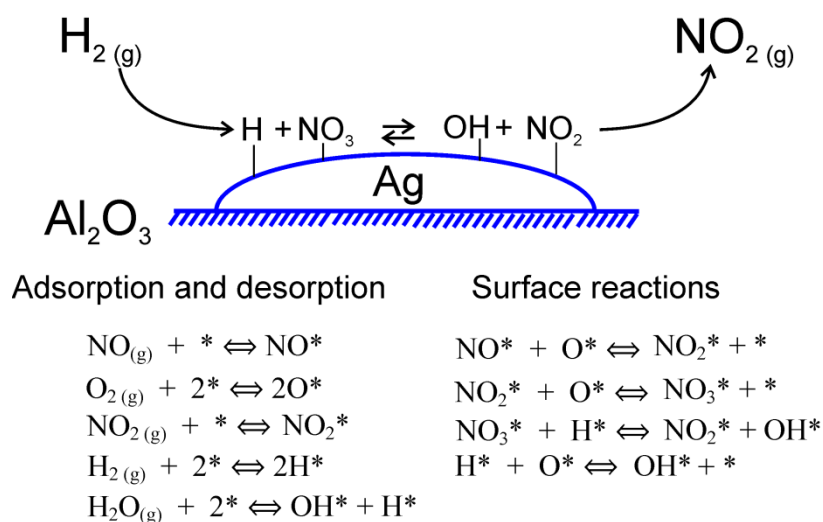


Figure 7.2 Schematic role of H₂ to promote NO oxidation and all elementary steps used in the model

An example of kinetic modeling results taken from a transient series at 400°C is shown in Figure 7.3. As seen here, the kinetic model used captured well the transient data of gas concentrations with correct trends and time-scale of responses. The activating role of H₂ by decreasing the surface nitrate coverage can be seen even at 400°C although this effect is not as high as at 250°C.

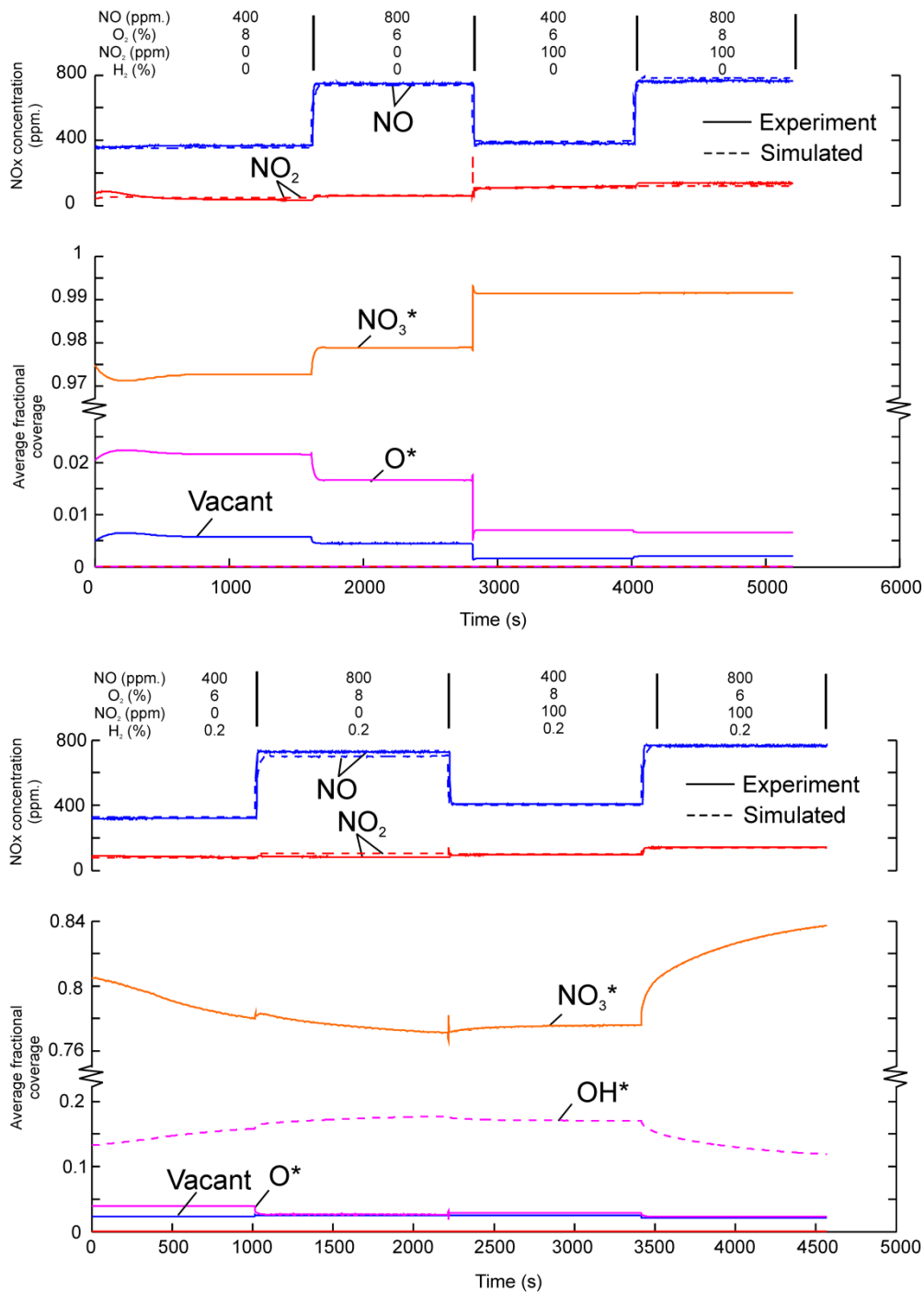


Figure 7.3 The experimental and simulation results from DOE experiment for varying feed concentration at 400°C.

Besides NO oxidation, H₂ oxidation to H₂O is an additional reaction that occurs when H₂ was fed. The nature of this reaction is fast and complete conversion of H₂ to H₂O was always observed already at 250°C which is also confirmed by the model. According to the model prediction of the H₂ concentration profile, the H₂ concentration decreased rapidly at the front part of monolith to form water due to its fast reaction. In addition, the model predictions as well as calculation of a Weisz modulus indicated the importance of internal transport limitations for diffusion of H₂ into the washcoat.

Instead of considering only the average surface coverage throughout the monolith, the current reactor model also allowed an analysis of the local surface coverage axially along the monolith as well as through the washcoat depth for each measurement time. In addition, the distribution profile of gaseous components both throughout the washcoat and axially through the gas phase could be analyzed.

According to the modeling results, the enhancing effect of H₂ to reduce surface nitrate was isolated to a relatively small portion of the catalyst due to the fast reaction rate of H₂ oxidation (nearly 100% conversion for all experiments in this study) suggesting that internal transport resistance may play a role even for H₂-assisted HC-SCR with Ag-Al₂O₃. At high temperature, the effect of transport resistance was more prevalent causing the portion of the catalyst affected by H₂ to be even smaller. In the absence of H₂ in the feed, the gradient of nitrate coverage in the front part of monolith disappeared and the nitrate coverage became equal throughout the catalyst.

7.3 Kinetic modeling of H₂-assisted C₃H₆-SCR (Paper III)

Paper III presented a global kinetic model to describe the role of H₂ to enhance NO oxidation and C₃H₆-SCR. The overall objective here was to propose an effective global kinetic model for C₃H₆-SCR based on a mechanistic representation of the promotional effect of H₂. A global kinetic model was developed successively based on experiments consisting of temperature-programmed reaction (TPR) and transient series experiments, covering a comprehensive set of inlet conditions. Reaction conditions used for model development included: NO oxidation, C₃H₆ oxidation and C₃H₆-SCR with and without H₂. In addition, the proposed model not only simulates the reaction kinetics but also all relevant mass transport resistances in the monolith reactor.

As mentioned earlier (Chapter 3), multiple roles for the promotional effect of H₂ on HC-SCR have been described. Considering the many possible roles of H₂ suggested in the literature, it is difficult to develop a kinetic model containing a comprehensive representation of the promoting role(s) of H₂. However, one could broadly summarize the literature by saying that H₂ has been suggested to have at least two overall roles; influencing surface coverages of most notably nitrates and oxygenated hydrocarbon intermediates and modifying/forming new more active sites. Thus, the global kinetic model presented here was intended to at least contain a representation of these dual general roles of H₂. It has also been widely reported that the role of H₂ involves the formation of reactive species or intermediates. However, these may simply be a consequence of the H₂ effect and linked to higher SCR activity.

In the previous section (7.2), a microkinetic model for H₂-assisted NO oxidation was described. It was based on the single role of H₂ to decompose nitrates over one type of site, however for a limited range of temperature. Initial kinetic model screening during model development indicated that a model based on a single role of H₂ to remove inhibiting

nitrates was insufficient to well reproduce all experimental data studied here, for two reasons:

- From the NO oxidation and C₃H₆-SCR experimental data, NO₂ yield and NO_x conversion are higher in the presence of H₂ over the entire temperature range, even at the highest temperature of 500°C (NO₂ yield and NO_x conversion were ca. 132% and 108% higher respectively). Nitrate poisoning should play a diminishing role at higher temperature where activities with and without H₂ eventually become equal.
- For the current data in addition to NO oxidation, there is C₃H₆ oxidation and C₃H₆-SCR reactions which are also affected to different degrees by the presence of H₂ as illustrated for NO oxidation and C₃H₆-SCR in the point above.

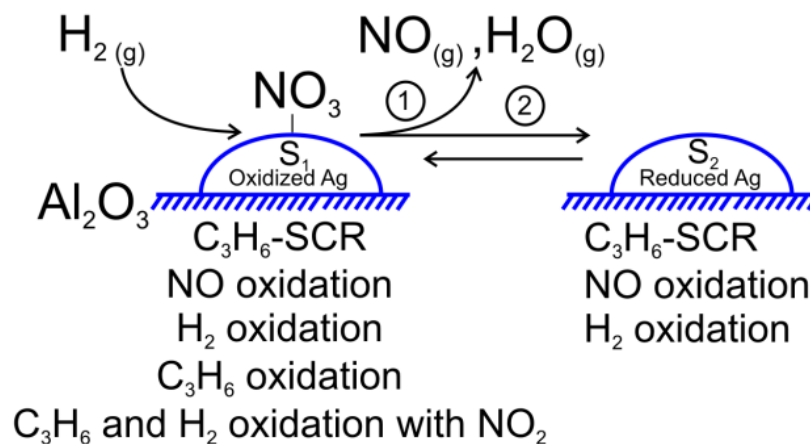


Figure 7.4 Schematic representation of reaction mechanism used in the present model

Figure 7.4 presents a schematic diagram of the reaction mechanism used in the final model. For site designation, S₁ can be regarded as oxidized Ag sites while S₂ represents reduced Ag sites. The dual roles of H₂ were to remove inhibiting nitrates from S₁ and in parallel to form a new site, S₂. Formation of S₂ is promoted by H₂ and is thus more active than S₁ for NO and H₂ oxidation as well as C₃H₆-SCR reactions. In the model, addition of NO_x initiates formation of poisoning nitrates over S₁ denoted as S₁-NO₃. The proposed reaction mechanism shown by Figure 7.4 is intended to be able to replicate the following features of the experimental results:

- NO oxidation and C₃H₆-SCR would be promoted by H₂ due to removal of poisoning nitrates from S₁ and the simultaneous generation of S₂.
- C₃H₆ oxidation will be inhibited for experiments with NO feed by nitrates on S₁. However, in the presence of NO and H₂ feed, C₃H₆ consumption will increase due to removal of nitrates from S₁ that gives higher C₃H₆ oxidation and generation of S₂ that is more active for C₃H₆-SCR.
- For experiments with NO feed, H₂ consumption will be greater because it removes nitrates from S₁ and generates S₂.

- At higher temperatures, C₃H₆ and H₂ oxidation by NO₂ will occur over S₁.

Table 7-2 presents the reactions used in the final model including two types of active sites, S₁ and S₂. To keep the model as simple as possible, first order reactions with respect to each reactant, surface species or site vacancy were assumed for reaction rates. For all reactions that were intended to occur on a site, their rates were set proportional to the quantity of that site (e.g. S₂) or the quantity of the vacant site (S₁ free of nitrate). Sites were conserved by the following balance, fulfilled by the model:

$$\theta_{S_1} + \theta_{S_1-NO_3} + \theta_{S_2} = 1 \quad (7.1)$$

Further, for all reactions involving O₂ the reaction orders with respect to O₂ were lumped with the kinetic parameters. In addition, the reversible surface reactions of oxidized S₁ site to reduced S₂ site and vice versa (reactions 7 and 8 in Table 7-2) should also involve formation and consumption of oxygen. However, since the stoichiometries of these reactions are not exactly known, they are neglected. Since all experiments were always performed under conditions with a large excess of O₂, the changes in O₂ concentration due to reactions were small. As a result, neglecting oxygen formation/consumption has a negligible impact on the modeling results.

Table 7-2 Reaction mechanism and reaction rate used in the kinetic model

No.	Reaction	Reaction rate
<i>NO oxidation over S₁ and S₂</i>		
1a	$NO(g) + 0.5 O_2(g) \xrightleftharpoons{S_1} NO_2(g)$	$r_{1a} = k_{1a} \cdot \left(y_{NO} - \left(\frac{1}{Keq_{1,T}} \right) \cdot y_{NO_2} \right) \cdot \theta_{S_1}$
1b	$NO(g) + 0.5 O_2(g) \xrightleftharpoons{S_2} NO_2(g)$	$r_{1b} = k_{1b} \cdot \left(y_{NO} - \left(\frac{1}{Keq_{1,T}} \right) \cdot y_{NO_2} \right) \cdot \theta_{S_2}$
<i>H₂ oxidation over S₁ and S₂</i>		
2a	$H_2(g) + 0.5 O_2(g) \xrightarrow{S_1} H_2O(g)$	$r_{2a} = k_{2a} \cdot y_{H_2} \cdot \theta_{S_1}$
2b	$H_2(g) + 0.5 O_2(g) \xrightarrow{S_2} H_2O(g)$	$r_{2b} = k_{2b} \cdot y_{H_2} \cdot \theta_{S_2}$
<i>C₃H₆ oxidation over S₁</i>		
3	$C_3H_6(g) + 4.5 O_2(g) \xrightarrow{S_1} 3CO_2(g) + 3H_2O(g)$	$r_3 = k_3 \cdot y_{C_3H_6} \cdot \theta_{S_1}$
<i>C₃H₆ and H₂ oxidation with NO₂ over S₁</i>		
4	$NO_2(g) + H_2(g) \xrightarrow{S_1} NO(g) + H_2O(g)$	$r_4 = k_4 \cdot y_{NO_2} \cdot y_{H_2} \cdot \theta_{S_1}$
5	$9NO_2(g) + C_3H_6(g) \xrightarrow{S_1} 3CO_2(g) + 9NO(g) + 3H_2O(g)$	$r_5 = k_5 \cdot y_{NO_2} \cdot y_{C_3H_6} \cdot \theta_{S_1}$
<i>Surface reaction: nitrate formation and removal</i>		
6	$NO(g) + O_2(g) + S_1 \leftrightarrow S_1 - NO_3$	$r_6 = k_6 \cdot \left(y_{NO} \theta_{S_1} - \left(\frac{1}{Keq_{2,T}} \right) \cdot \theta_{S_1 - NO_3} \right)$ $\approx 0^+$ $Keq_{2,T} = \frac{\theta_{S_1 - NO_3}}{(y_{NO} \cdot \theta_{S_1})}$
7	$2 H_2(g) + S_1 - NO_3 \rightarrow NO(g) + 2H_2O(g) + S_2$	$r_7 = k_7 \cdot y_{H_2} \cdot \theta_{S_1 - NO_3}$
8	$S_2 \rightarrow S_1$	$r_8 = k_8 \cdot \theta_{S_2}$
<i>C₃H₆ SCR over S₁ and S₂</i>		
9a	$C_3H_6(g) + NO(g) + 4 O_2(g) \xrightarrow{S_1} 0.5N_2 + 3CO_2 + 3H_2O(g)$	$r_{9a} = k_{9a} \cdot y_{C_3H_6} \cdot y_{NO} \cdot \theta_{S_1}$
9b	$C_3H_6(g) + NO(g) + 4 O_2(g) \xrightarrow{S_2} 0.5N_2 + 3CO_2 + 3H_2O(g)$	$r_{9b} = k_{9b} \cdot y_{C_3H_6} \cdot y_{NO} \cdot \theta_{S_2}$

f) quasi-equilibrium imposed

The kinetic parameter fitting was carried out in stages, where parameters for reactions that were exclusive to experimental sets were fitted first. Then for experimental sets involving additional reactions, the additional parameters were successively fitted. A complete list of kinetic parameters can be found in **Paper III**. From statistical analyses, all kinetic parameters were found to be significant within 95% confidence intervals. An example of the results

from the proposed model for temperature-programmed reaction of H₂-assisted C₃H₆-SCR is shown in Figure 7.5

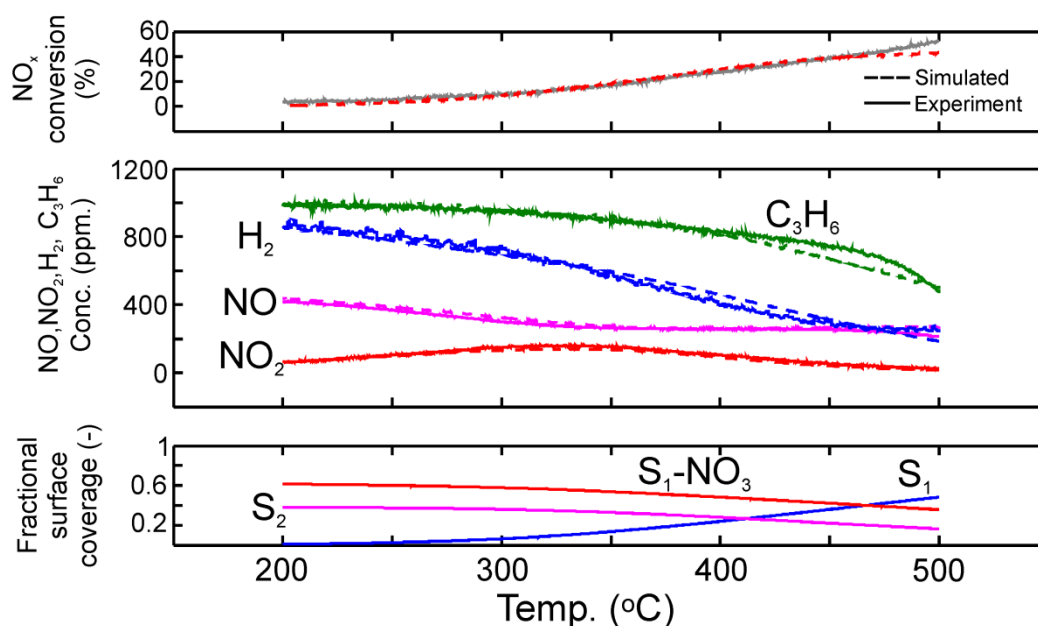


Figure 7.5 Comparison between simulation and experimental data for H₂-assisted C₃H₆-SCR. Inlet feed: 500 ppm NO, 1000 ppm C₃H₆, 8% O₂, 1000 ppm H₂, 5% H₂O.

The effect of varying C₃H₆ and H₂ concentrations

Transient experiments involving stepwise increasing C₃H₆ and H₂ concentrations were also conducted at 375°C. In the absence of H₂, the catalyst was inactive for SCR at this temperature and increasing C₃H₆ concentration did not promote SCR activity since NO_x conversion was always below 2%, as also predicted well by the model. C₃H₆ consumption and NO oxidation at this temperature were also negligible which is in agreement with the previous TPR data.

Figure 7.6a shows the effect of C₃H₆ on H₂-assisted C₃H₆-SCR. By increasing stepwise the C₃H₆ feed concentration, the resulting increase of NO_x conversion was captured well by the model. From the dynamics of the surface species, it was found that the changes in all surface species were negligible. These modeling results indicate that a first order dependence on C₃H₆ concentration for SCR as shown by reaction 9a and 9b in Table 7-2 appears satisfactory. Further, the model prediction for the activation energy of reaction 9b (ca. 64 kJ/mol) is lower than the SCR reaction on reaction 9a (ca.186 kJ/mol). From the dynamic changes in NO_x conversion and gas concentrations, it was apparent that the effect of increasing C₃H₆ concentration was immediate and the model reproduced this behavior well.

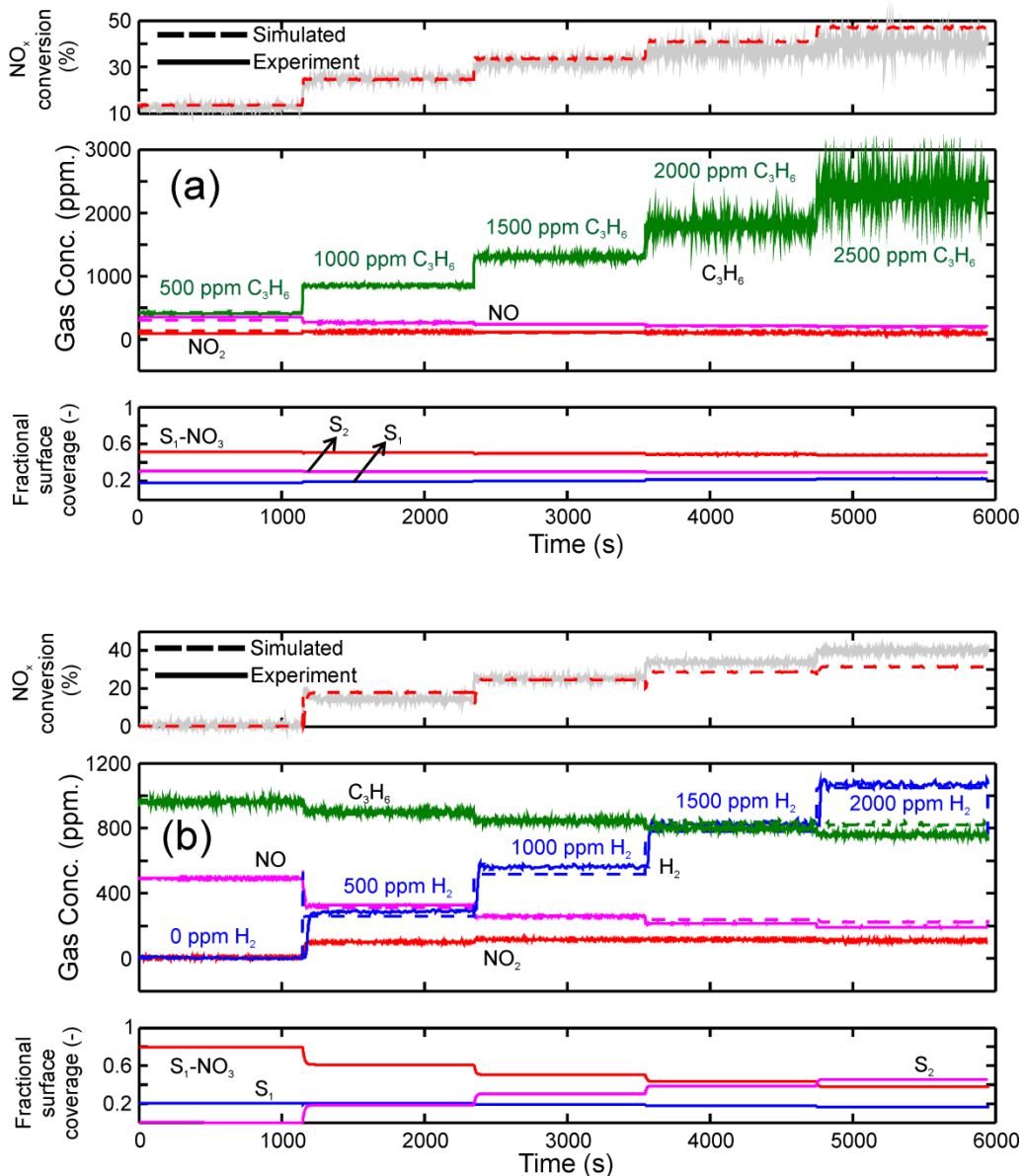


Figure 7.6 Comparison between simulation and experimental data to investigate the effect of varying C_3H_6 concentration for H_2 -assisted C_3H_6 -SCR (a, top panel) and varying H_2 concentration for H_2 -assisted C_3H_6 -SCR (b, bottom panel). Inlet feed: (a) 500 ppm NO , 500–2500 ppm C_3H_6 , 8% O_2 , 1000 ppm H_2 , 5% H_2O , (b) 500 ppm NO , 1000 ppm C_3H_6 , 8% O_2 , 0–2000 ppm H_2 , 5% H_2O .

Finally, the promotional effect of H_2 was examined by varying the H_2 feed concentration from 0 to 2000 ppm (Figure 7.6b). The increase in NO_x conversion is immediate along with higher H_2 concentration. They also resulted in higher S_2 coverages and lower nitrate coverage on S_1 (S_1-NO_3). However, the fractional vacancy of the site S_1 is nearly stable. As a result, the model predicts a higher reaction rate for H_2 -assisted C_3H_6 -SCR by reaction 9b due to higher availability of S_2 . Related to C_3H_6 consumption, a nearly constant S_1 and higher S_2 means that higher C_3H_6 consumption is almost exclusively due to higher SCR activity.

Evaluation of mass transport resistances

Discretization in both axial and radial direction facilitates an investigation of possible mass transfer effects for each measurement time. This is illustrated by Figure 7.7 showing a surface plot of NO concentration during H₂-assisted C₃H₆-SCR experimental conditions at 450°C.

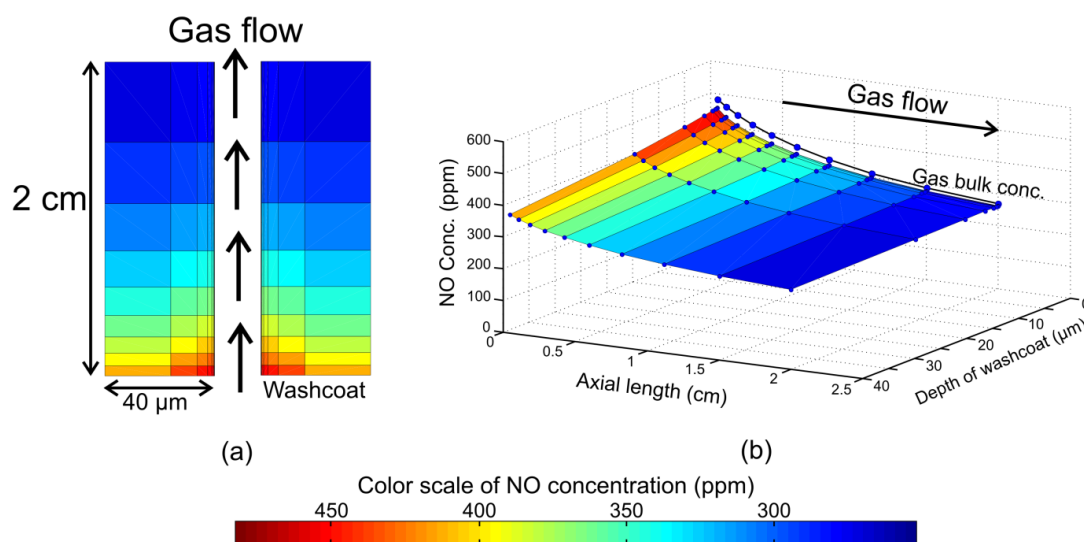


Figure 7.7 Bulk gas and washcoat NO concentration predicted by model at 450°C during H₂-assisted C₃H₆-SCR. (a) top view over monolith washcoat (unscaled dimensions) (b) bulk gas and surface plot over washcoat.

As shown here, NO concentration drops steadily in the axial direction as it is consumed via NO oxidation and SCR reactions. An NO concentration gradient through the depth of the washcoat of as much as 80 ppm is observable at the monolith inlet (Figure 7.7b). This indicates some influence of internal pore mass transfer resistance for NO at 450°C. For the same results at 200°C, an NO concentration gradient of only 8 ppm was observed which indicates that mass transfer resistance is stronger, as expected, at high temperatures.

To further evaluate internal mass transfer resistance as a function of temperature, the Weisz moduli were calculated for NO, C₃H₆ and H₂ during H₂-assisted C₃H₆-SCR as well as C₃H₆-SCR. The results of calculation for H₂-assisted C₃H₆-SCR were plotted in Figure 9 of **Paper III**. Under H₂-assisted C₃H₆-SCR conditions, NO was found to be mildly influenced by internal mass transfer between 250-500°C. While calculations for C₃H₆ and H₂ under the same conditions showed that only a small portion of the data (notably above 400°C) were influenced by mass transport resistance. Similar analyses for NO and C₃H₆ under C₃H₆-SCR condition indicated that the influence of internal mass transfer only played role at high temperature above 436°C. Since mass transport resistance was found to be important at higher temperature and under specific reaction conditions, it can be concluded that a larger fraction of experimental data gathered in the present study was nevertheless free from the influence of mass transport resistances.

Surface species quantification as a support for SCR modeling

Kinetic models to describe the effects of H₂ to promote NO oxidation and C₃H₆-SCR over Ag/Al₂O₃ catalysts have been constructed in Chapter 7. In the kinetic model of **Paper III**, dual roles of H₂ were proposed to facilitate removal of nitrate as well as formation of more active Ag sites. These two key factors enabled simulation of NO oxidation and C₃H₆-SCR cases for a wide variety of feed mixtures and temperatures.

In addition, temperature-programmed desorption (TPD) studies of NO_x over Ag/Al₂O₃ and Al₂O₃ as a way to probe nitrate species formed on the catalyst have been presented in Chapter 6 / **Paper I**. There, the dual roles of H₂ to influence nitrate species were verified. It was shown that H₂ played a role in removing inhibiting nitrate on active sites as well as to facilitate storage of inactive nitrate species mainly on the catalyst support. Hence, it is of interest to envisage the applicability of TPD experiments to provide an estimate of surface NO_x quantity, which thus may improve the existing C₃H₆-SCR kinetic model in **Paper III**.

8.1 Experimental estimation of surface NO_x species using TPD technique

A series of TPD experiments have been conducted as a way to estimate the amount of various nitrate species over Ag-Al₂O₃ catalyst based on similar TPD protocols conducted previously in **Paper I**. Figure 8.1 shows the NO_x desorption peaks during temperature ramps (desorption step) that were preceded by adsorption treatments with NO oxidation and H₂-assisted NO oxidation. The previous TPD studies in **Paper I** showed that there were 2 easily discernible types of NO_x desorption peaks, identified as low temperature and high temperature peaks. As seen in Figure 8.1 for NO oxidation pretreatments, the NO_x desorption peaks assignable to low temperature and high temperature peaks were not clearly distinguishable. Therefore, a fitting procedure to separate NO_x desorption peaks was carried out using an open access *peakfit* function in Matlab [105]. The results from the peak-fitting procedure using Gaussian functions are also presented in Figure 8.1.

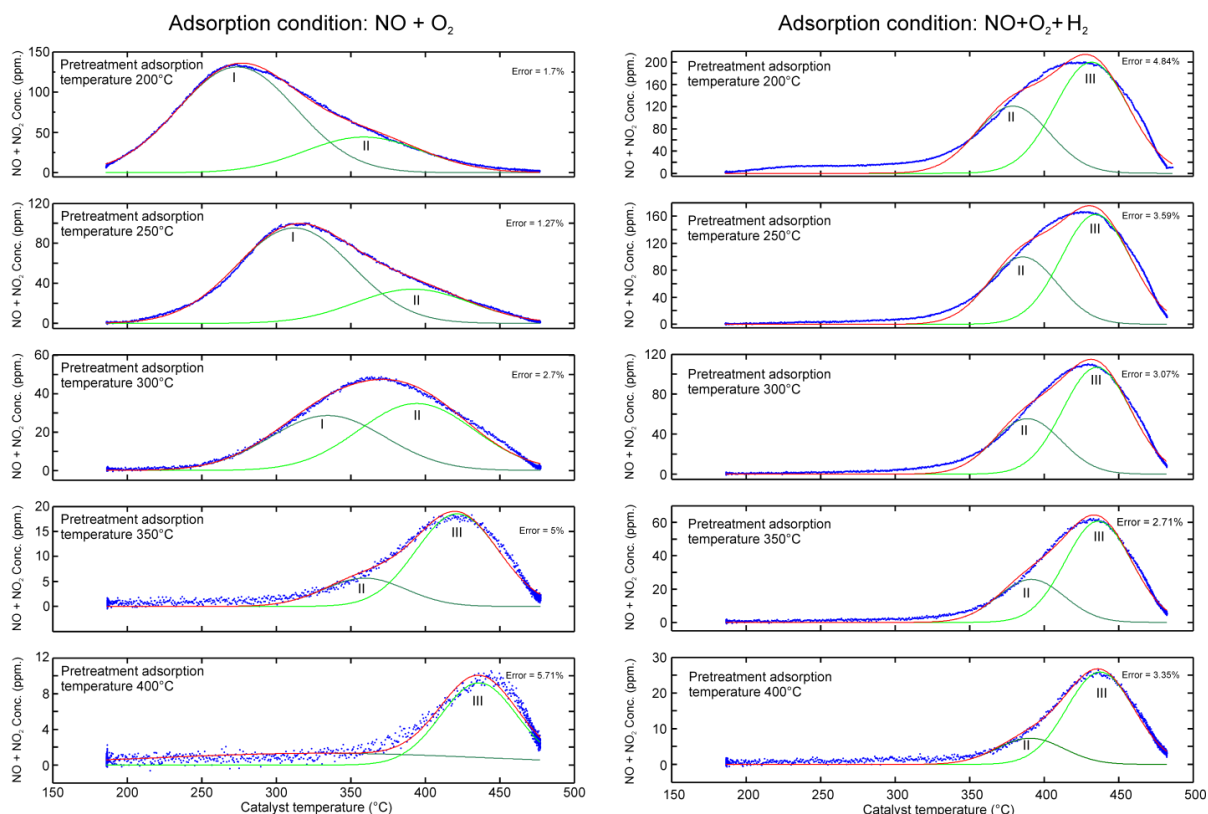


Figure 8.1 Deconvolution of NO_x desorption peaks over 2 wt.% $\text{Ag-Al}_2\text{O}_3$ during temperature ramp in Ar flow. The plots show the raw data (blue), fitted functions (red) and deconvoluted peaks (green). Preceding adsorption conditions are: 500 ppm $\text{NO}+8\%\text{O}_2$ (left panels) or 500 ppm $\text{NO}+8\%\text{O}_2+0.1\%\text{H}_2$ (right panels).

The results from peak fitting of NO_x desorption peaks (Figure 8.1) identified the presence of 3 types of surface NO_x species denoted as peak I, peak II and peak III, respectively. Integration of each peak yielded the amount of NO_x species (in $\mu\text{mol.g}^{-1}$) and is displayed in Table 8-1. For comparison, the concentration of atomic Ag in 2 wt.% $\text{Ag-Al}_2\text{O}_3$ catalyst is $185 \mu\text{mol.g}^{-1}$.

Figure 8.1 and Table 8-1 show that peak I and peak II are the dominant desorption peaks following NO oxidation pretreatment. Whereas, peak II and peak III are the only desorption peaks observed following H_2 -assisted NO oxidation. As shown in Table 8-1, the quantity of NO_x desorbed in all peaks generally decreased with higher adsorption temperatures.

Table 8-1 Approximation of NO_x quantities during desorption step shown in Figure 8.1

Adsorption temperatures with NO+O ₂ pretreatment	Peak I (μmol.g ⁻¹)	Peak II (μmol.g ⁻¹)	Peak III (μmol.g ⁻¹)
200°C	44.4	15.2	-
250°C	31.9	11.3	-
300°C	9.6	11.5	-
350°C	-	1.3	4.3
400°C	-	-	1.9

Adsorption temperatures with NO+O ₂ +H ₂ pretreatment	Peak I (μmol.g ⁻¹)	Peak II (μmol.g ⁻¹)	Peak III (μmol.g ⁻¹)
200°C	-	25.7	41.9
250°C	-	20.1	32.1
300°C	-	10.9	20.6
350°C	-	5.0	11.5
400°C	-	1.4	4.9

8.2 Interpretation of surface NO_x species to give insights for mechanistic study

With the addition of H₂, the NO oxidation activity over the Ag/Al₂O₃ catalyst is largely promoted nearly at all temperatures as shown in Figure 3.2b. It is thus of interest to relate the results from the TPD in Figure 8.1 with the mechanistic study of H₂-assisted NO oxidation or H₂-assisted C₃H₆-SCR. As suggested in Figure 8.1, there are 3 types of surface NO_x species that can be related to nitrate species (see DRIFTS results on Figure 6.3). Peak I observed in Figure 8.1 could be associated to the low temperature peak as observed in Figure 6.1, which implies that this peak can then be attributed to the nitrate species located on the active part of the catalyst.

Addition of H₂ caused a notable increase in the quantities of peak II and peak III (Table 8-1). As a result, peak II and peak III can then be related to the high temperature peak previously observed in Figure 6.1. These peaks are likely to originate from the decomposition of inert nitrate species mainly on the Al₂O₃ support.

As addressed in the beginning of this chapter, it is of interest to demonstrate the applicability of NO_x TPD in Figure 8.1 as a way to improve the kinetic model of C₃H₆-SCR. Experimental estimation of surface species would help the model to better predict the quantity of surface species. To implement this, a residual calculation for the quantity of surface species can be included in addition to the residual calculation for gas composition in the objective function of the parameter estimation for the kinetic model.

Paper II and **III** addressed that one crucial role of H₂ in improving low temperature activities of SCR and NO oxidation is to eliminate inhibiting nitrate species *viz.* peak I. With the aid of the current model in **Paper III**, kinetic parameters describing elimination of peak I by H₂ can be re-tuned to follow the same trend as in Table 8-1. Similarly, the increase in NO oxidation

conversion with the increase in temperature can also be explained by the decrease of peak I.

In addition, the quantification of NO_x storage based on peaks II and III in Figure 8.1 may also serve as a basis to reveal the mechanism of H₂-induced NO_x storage on Ag/Al₂O₃ catalyst. As addressed earlier, these peaks are attributable to the nitrate species probably on the Al₂O₃ support. A mechanistic study of the storage process for instance through a readsorption or spill-over mechanism can be envisaged from a modeling point of view. From literature, the concept of NO_x storage and reduction (NSR) over Ag/Al₂O₃ catalysts with the aid of H₂ to abate low temperature NO_x emission has been recently reported by Tamm et al [106, 107] as well as by a group at General Motors [108]. Therefore, a mechanistic study of the H₂ effect on the NO_x storage mechanism will also be advantageous for development of possible NSR processes involving a Ag/Al₂O₃ catalyst.

Evaluation of the H₂ effect on DOC

Addition of H₂ as a way to improve the NO oxidation activity over DOC has been presented by Herreros et al. [22] in an engine bench study. In order to gain a deepened insight into H₂ effects on DOC, a systematic investigation on a lab-sized monolith supported Pt/Al₂O₃ catalyst was performed as presented in **Paper IV**. The effect of CO and C₃H₆ in the inlet feed, combined with different concentrations of H₂, was investigated. In addition, transient experiments with H₂ switched in and out of the feed were also conducted to identify the time scale of the H₂ effect with various gas mixtures. Eventually, the surface chemistry and exothermal heat effect due to H₂ addition could also be discriminated.

9.1 The effect of H₂ with various gas mixtures

In order to investigate the effect of H₂ on Pt/Al₂O₃, activity measurements using temperature-programmed reaction (TPR) experiments were conducted. Table 9-1 displays the synthetic exhaust gas inlet compositions used in the TPR experiments.

Table 9-1 Synthetic exhaust gas composition used with varied H₂ concentrations (0,250,...,1000 ppm).

Gas mixture notation	Inlet composition
NO/O ₂	500 ppm NO, 8% O ₂ , 5% H ₂ O
NO/O ₂ /CO	500 ppm NO, 8% O ₂ , 200 ppm CO, 5% H ₂ O
NO/O ₂ /C ₃ H ₆	500 ppm NO, 8% O ₂ , 200 ppm C ₃ H ₆ , 5% H ₂ O
NO/O ₂ /CO/C ₃ H ₆	500 ppm NO, 8% O ₂ , 200 ppm C ₃ H ₆ , 200 ppm CO, 5% H ₂ O

Prior to each experiment, a pretreatment was conducted to obtain a Pt oxide free surface over the catalyst. For this purpose, the catalyst was exposed consecutively to the following oxidative and reductive dry atmospheres at 450°C:

- 10% O₂ in Ar (balance in all experiments) with duration of 20 min.
- 2% H₂ in Ar with duration of 30 min.

Figure 9.1 shows the results of the H₂ effect on NO oxidation as a function of catalyst temperature with various gas mixtures, during TPR heating ramps that were preceded by

catalyst pretreatment and inert cooling steps. The “catalyst temperature” here is a measure of the temperature near the outlet end of the monolith. Despite the presence of oxidation reactions that caused increased axial temperature gradients, the use of catalyst temperature should in fact provide a very modest estimate of any promotional effects of H₂ minus exothermal heat effects.

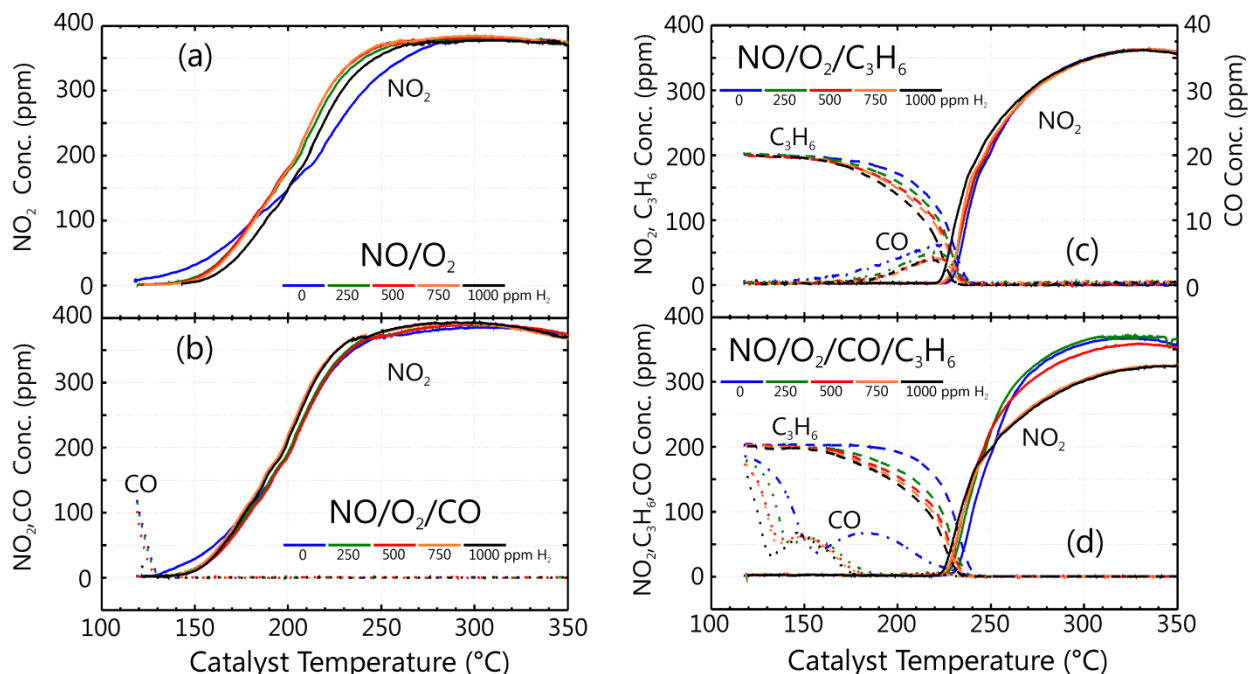


Figure 9.1 The effect of H₂ concentration on NO oxidation over Pt/Al₂O₃ with various gas mixtures during heating ramp following pretreatment of the catalyst. Total flow of 3000 ml/min was used with Ar balance equivalent to GHSV of ca. 29000 h⁻¹ or WHSV of 562 h⁻¹. See table 9.1 for inlet feed condition.

Generally, the effect of H₂ on the NO₂ yield varied, depending upon the temperature region and feed H₂ concentration. Measurement of the H₂ signal (not shown) indicated that H₂ was generally already fully converted by 200°C in all cases, even with the highest H₂ concentration. It is also noteworthy that above 300°C, the NO₂ yield should be limited by thermodynamic equilibrium as reported in [19]. The onset of equilibrium is evident in Figure 9.1 for all gas mixtures by the leveling off and even eventual decrease in NO₂ yields at temperatures above 300°C.

Figure 9.1a shows the result for the NO/O₂ mixture where addition of H₂ had both negative and positive effects on the NO₂ yield. At low temperature (below 200°C), addition of H₂ lowered the NO₂ yield. However, between 200-300°C, H₂ was found to enhance the NO₂ yield in this mixture. Additionally, it was also found that addition of H₂ up to 750 ppm improved the NO₂ yield, however with 1000 ppm H₂ the NO₂ yield started to decrease.

Figure 9.1b shows the result for the NO/O₂/CO gas mixture. It was observed that H₂ had little effect on the NO₂ yield, although a marginal increase in the NO₂ yield could still be

seen between 180-300°C with higher H₂ concentration. Addition of H₂ also lowered the temperature to attain complete CO conversion from ca. 135°C in the absence of H₂ to ca. 126°C in the presence of 1000 ppm of H₂.

As shown in Figure 9.1c for the NO/O₂/C₃H₆ mixture, a strong inhibition effect of C₃H₆ on the NO oxidation was observed by the delayed light-off for NO oxidation to at least 220°C. Addition of H₂ was however found to decrease the light-off temperature as well as to increase the NO₂ yield within a temperature range of 220-325°C. As the onset for C₃H₆ conversion started, there was also detectable formation of CO which was probably due to partial oxidation of C₃H₆.

Eventually, the effect of H₂ was also investigated on a complete mixture of NO/O₂/CO/C₃H₆ (Figure 9.1d). An increase of the H₂ concentration was found to decrease the light-off temperature for NO, C₃H₆ and CO oxidation. Further, addition of low amounts of H₂ such as 250 ppm H₂ was found to be beneficial for the NO₂ yield in the temperature range above 220°C. Addition of higher H₂ concentrations, however, gave a lower NO₂ yield above 240°C. The detrimental effect of H₂ was most prominent with H₂ concentrations of 750 and 1000 ppm.

9.2 The effect of H₂ to influence hysteresis

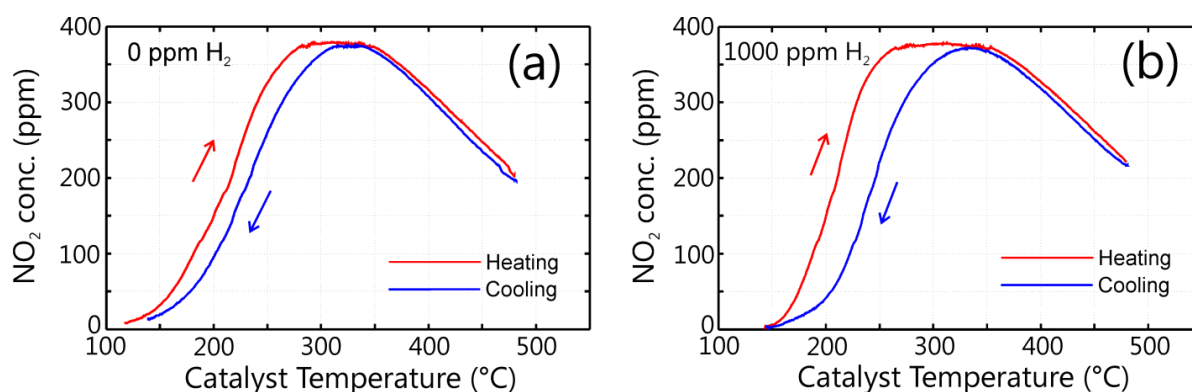


Figure 9.2 The effect of H₂ to influence the hysteresis of NO oxidation over 1 wt.% Pt/Al₂O₃ catalyst.

As addressed in Chapter 3, the hysteresis phenomenon during NO oxidation over Pt/Al₂O₃ is commonly reported in literature. In connection with hysteresis, PtO formation is often proposed as the reason behind different activities during heating and cooling ramps [15]. Figure 9.2 demonstrates the results of TPR from heating and cooling ramps during NO oxidation reaction over Pt/Al₂O₃ with and without H₂. As seen here, addition of 1000 ppm of H₂ altered the heating and cooling curves (Figure 9.2b), which resulted in a broadened hysteresis loop compared to that in the absence of H₂ (Figure 9.2a).

9.3 Transient NO_2 yields at constant temperature

It has been shown in literature that the NO oxidation conversion decreases as a function of time due to the gradual build-up of Pt oxide [13]. In connection to the H_2 promotional effect, it was therefore of interest to investigate if H_2 may influence the decay in the NO oxidation activity as well as the dynamic effect of H_2 to influence NO oxidation in various mixtures.

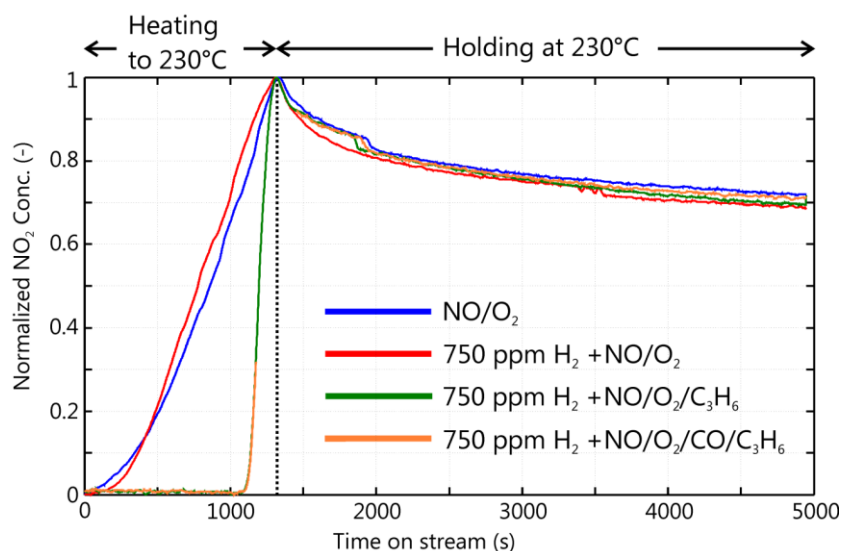


Figure 9.3 The evolution of the normalized NO_2 signal for various gas mixtures as a function of time. The reactor was heated from 120 to 230°C and held constant at 230°C for 1h.

Figure 9.3 presents the evolution of the normalized NO_2 signal for various gas mixtures as a function of time. The NO_2 signal was rescaled to the values within a range of 0 to 1 by normalization based on the maximum and minimum NO_2 outlet signals over the time range. As seen here, when the temperature was held constant, there was a substantial decrease in the NO_2 signal as it dropped by as much as 30% from its maximum value. A comparison of the NO/O_2 mixture with the other H_2 -containing gas mixtures, shows that the rate of decay of the NO_2 yields were similar. In fact, there was a slightly faster rate of decrease in NO_2 observed for NO/O_2 with H_2 compared to without H_2 .

9.4 Transient experiments with in/out H_2 switching

To determine the dynamic effect of H_2 with various gas mixtures, transient experiments involving switching in/out H_2 were conducted and the results are presented in Figure 9.4. Similar to Figure 9.3, generally one can still observe a decline in the NO_2 signal as a function of time for all gas mixtures, despite the periodic switching of H_2 . MS measurements indicated that H_2 was always fully converted in all cases.

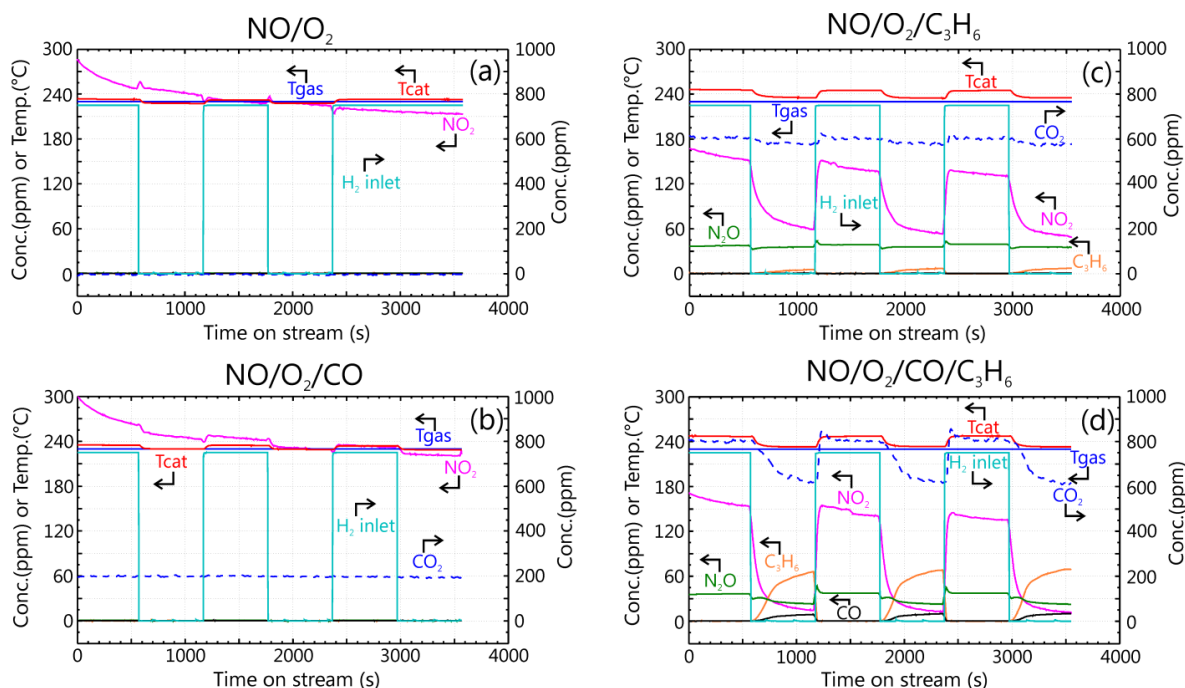


Figure 9.4 The dynamic effects of switching in and out 750 ppm of H₂ with different gas mixtures (see Table 9-1). The catalyst was previously exposed to TPR by cofeeding 750 ppm of H₂ with corresponding gas mixture from 120 to 230°C and held constant at 230°C.

Introduction of 750 ppm of H₂, clearly caused the catalyst temperature (T_{cat}) to increase for all gas mixtures (Table 9-2). The temperature rise was naturally due to the exothermal H₂ combustion and was most prominently observed for the C₃H₆ containing mixtures. Therefore, the response of the NO₂ signal due to switching H₂ feed on and off, is due not only to possible effects of H₂ on surface chemistry and reactions but also to the temperature variations.

Table 9-2 Catalyst temperatures during exposure of catalyst intermittently with 750 ppm H₂ with set point inlet gas temperature of 230°C

Gas mixtures	Approximate catalyst temperature (°C)	
	without H ₂	with 750 ppm H ₂
NO/O ₂	227-228	232-233
NO/O ₂ /CO	228-230	234-235
NO/O ₂ /C ₃ H ₆	235-237	245-246
NO/O ₂ /CO/C ₃ H ₆	233	247-248

For the NO/O₂ mixture (Figure 9.4a), feeding in H₂ generally caused a lower NO₂ yield, which is contrary to the corresponding TPR results (Figure 9.1a). In contrast to the effect of H₂ on the NO/O₂ mixture, the effect of H₂ on the NO/O₂/CO mixture was found to be positive by giving higher NO₂ yields in the presence of H₂ (Figure 9.4b). In addition, complete conversion of CO was always observed under these conditions as indicated by the CO₂ signal.

The dynamic effect of H₂ on C₃H₆ containing gas mixtures is shown in Figure 9.4c and d. Addition of H₂ in these cases caused a notable increase not only in the NO₂ yield but also a slight increase in N₂O formation. It could also be seen that the effect of H₂ was almost instantaneous on the NO₂ yield when switched in, however, when switched out it declined more slowly over about 5 min, nearly following the decline in the catalyst temperature. For the NO/O₂/C₃H₆ mixture (Figure 9.4c), a remarkable increase in the NO₂ yield from 60 ppm to ca. 150 ppm could be observed in the second H₂ switch cycle (at ca. 1200 s). Observation at the same transient time for the NO/O₂/CO/C₃H₆ mixture indicates that addition of H₂ increased the NO₂ yield from 15 ppm to ca. 150 ppm (Figure 9.4d). From Figure 9.4c and d, complete conversion of C₃H₆ was always observed in the presence of H₂, whereas in the absence of H₂, C₃H₆ was detected in the outlet stream. The same also applies for CO in the NO/O₂/CO/C₃H₆ mixture as depicted in Figure 9.4d.

9.5 Discrimination of heat and chemical effects due to addition of H₂

The transient results presented in Figure 9.4 can also be used to probe the characteristics of the H₂ effect by comparing the response times for the NO₂ yield and catalyst temperature. Figure 9.5 shows the response of normalized NO₂ yields, H₂ feed and catalyst temperature upon introduction of H₂. Each of the values was rescaled in the range of 0 to 1 by normalization based on their maximum and minimum values within the time range. Additionally, a minor time lag between FTIR and temperature measurements was neglected.

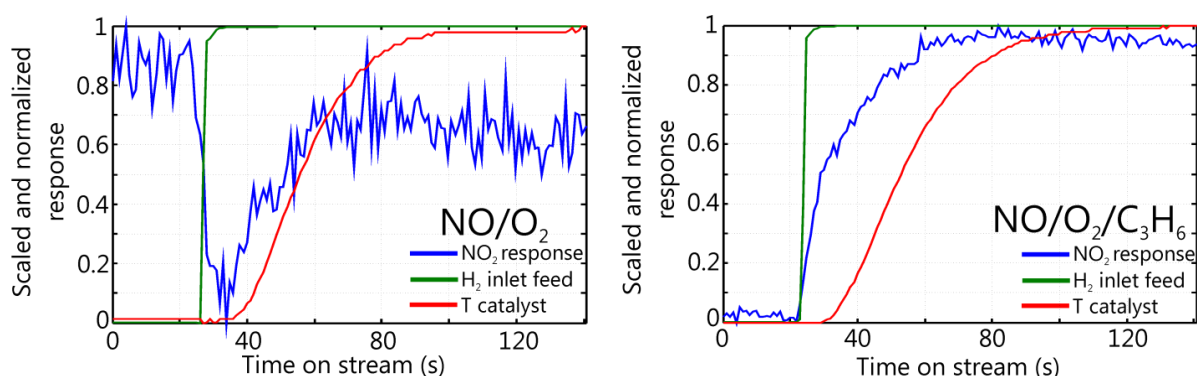


Figure 9.5 The normalized NO₂, H₂ feed and catalyst temperature signals from the second cycles (ca. 1200 s) in Figure 9.4 with corresponding gas mixtures.

As presented in Table 9-2, the increase in the catalyst temperature was due to the exothermal heat from H₂ combustion, but also in some cases the increased oxidation of CO and C₃H₆ caused by the H₂ feed. However it started to increase only about 15 s after the start of H₂ feed, due to the thermal inertia of the catalyst, monolith and glass tube encasing the monolith.

For both NO/O₂ (Figure 9.5 left panel) as well as NO/O₂/CO mixtures (see Figure 9 in **Paper IV**), the NO₂ signal first decreased when H₂ feed started and then it increased at about the same rate as temperature began to increase. The negative effect on the NO₂ yield

immediately following H₂ feed, indicated the presence of a rapid chemical effect which lowered the NO₂ yield. Subsequently, the gradual increase in NO₂ in parallel with the temperature increase indicated that this NO₂ increase was most likely merely resulting from heat effects.

However, for both NO/O₂/C₃H₆ (Figure 9.5, right panel) and NO/O₂/CO/C₃H₆ (see Figure 9 in **Paper IV**) mixtures, the NO₂ signal immediately increased when the H₂ feed was switched in. Afterwards, the NO₂ continued to increase along with the catalyst temperature. Again, the immediate increase of NO₂ along with H₂ feed shows the presence of H₂ chemical effects that beneficially alter surface species or reactions to increase the NO₂ yield.

9.6 Influence of H₂ on Pt oxide formation

It is generally accepted that Pt oxide formation is the phenomenon causing hysteresis behavior of NO oxidation over Pt/Al₂O₃ during TPR experiments [15]. With the aid of Figure 9.2, one can observe that addition of H₂ modified the hysteresis behavior. This implies that H₂ likely plays a role to influence Pt oxide formation. The extent of Pt oxide formation and the resulting hysteresis is reported to be related to the amount of NO₂ at medium and high temperatures near the thermodynamic equilibrium [15, 109]. This is due to the strong oxidative power of NO₂ to promote Pt oxide formation [13].

As seen from Figure 9.1a for the NO/O₂ mixture, addition of H₂ improved the NO₂ yield in the temperature range of 200-300°C. Improvement of the NO₂ yield can be associated with H₂ preventing the formation of inactive Pt oxide over the catalyst. Deactivation due to Pt oxide formation is obviously a slow process, occurring on the scale of several minutes as illustrated by Figure 9.3. Also, at least at 230°C, it occurs for all of the gas mixtures with or without H₂. It is likely then that H₂ hinders Pt oxide formation during the TPR, only at low temperatures, mostly below 200°C, when H₂ conversion was less than complete. However, at temperatures above 200°C, Pt oxide starts to form towards the rear part of the monolith which is no longer exposed to H₂, but is required for NO oxidation. The result is that the promotion of NO₂ formation with H₂ during the TPR with the NO/O₂ mixture was a temporary effect. It results from H₂ retarding Pt oxide formation at low temperature and the rate of Pt oxide formation lagging behind that of the temperature increase. As illustrated by Figure 9.3 and Figure 9.4a, when the temperature ramp was stopped at 230°C, the Pt oxide formation was able to catch up and overtake the effect of the temperature increase. For operation at 230°C (Figure 9.4a), there was no longer any benefit remaining from any earlier retardation of Pt oxide formation. In addition, the transient experiment with NO/O₂ (Figure 9.5) also demonstrated that switching in H₂ gave an immediate decrease in the NO₂ yield, which was probably due to H₂ reacting with NO₂ facilitated by the catalyst.

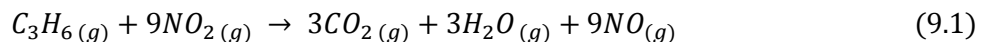
The results from Figure 9.1 also indicate that the presence of CO in the absence of H₂ generally gave higher NO₂ yield for NO/O₂ as in agreement with [15]. Similar to H₂, this enhancement effect of CO on NO oxidation is presumably due to the role of CO to retard Pt

oxidation at low temperature below 135°C when CO was still detectable in the outlet stream [15, 21]. With the relatively low CO concentration used here (200 ppm), it appears from comparison of Figure 9.1a and Figure 9.1b that CO has only a weak inhibition effect on NO oxidation. When H₂ and CO coexist, it is apparent that both species share the same function to retard Pt oxide formation. As a result, addition of H₂ to the NO/O₂/CO mixture resulted in only a marginal increase in the NO₂ yield. The addition of H₂ at 230°C to NO/O₂/CO (Figure 9.4b) had only a minor influence on the NO₂ yield. An immediate negative effect of H₂ on NO₂ yield can be due to surface reaction between H₂ and NO₂.

9.7 H₂ influence on C₃H₆ and CO oxidation and interactions with NO oxidation

In C₃H₆ containing mixtures, it is evident that C₃H₆ has a strong inhibition effect on NO oxidation at low temperature, before the onset of C₃H₆ oxidation (Figure 9.1c and d). Addition of H₂ was found to weaken the inhibition effect of C₃H₆ by lowering the light-off temperature for C₃H₆ oxidation which in turn promoted NO oxidation. It is also notable that C₃H₆ caused the light-off temperature for CO oxidation to increase approximately 25°C. In contrast, the first detection of NO₂ formation was delayed by about 100°C or until almost complete conversion of C₃H₆ was obtained. This demonstrates how C₃H₆ has a considerably larger inhibiting effect on NO oxidation than CO oxidation. In contrast, the effect of CO to inhibit C₃H₆ conversion through competitive adsorption was also small probably due to the low concentration of CO used here.

It has been suggested that C₃H₆ inhibits NO oxidation by reaction of C₃H₆ with NO₂ to form NO particularly at low temperatures [20, 110] as illustrated in the reaction below:



There is also the possibility that C₃H₆ preferentially adsorbs on sites and thus blocks both NO and CO oxidation. Undoubtedly both of these inhibition mechanisms play a role. However, considering that C₃H₆ has a much stronger inhibition effect on NO oxidation rather than on CO oxidation, the reaction of C₃H₆ with NO₂ into NO would probably appear to be the more prominent cause of C₃H₆ inhibition on NO oxidation.

From the transient experimental results with NO/O₂/C₃H₆ and NO/O₂/CO/C₃H₆ mixtures in Figure 9.4 and Figure 9.5, it appeared that the H₂ effect to improve NO₂ yield was instantaneous. The transient data also confirms that H₂ activates C₃H₆ oxidation and thereby promotes the NO oxidation reaction. Interestingly, the increase in NO₂ signals were found to be faster than that of temperature, suggesting that H₂ affected adsorbed species and surface reactions in addition to the exothermal effect due to its combustion (Figure 9.5). As addressed earlier, the effects of H₂ here can then be related to a decreased blocking effect of adsorbed C₃H₆ species and prevention of the reaction of C₃H₆ with NO₂ forming NO.

The inhibition effect of CO on NO oxidation, as shown in [15], cannot be fully demonstrated in Figure 9.1b probably due to the relatively low amount of CO used here (200 ppm of CO).

As shown in Figure 9.1b, addition of H₂ promotes CO oxidation by lowering the temperature for complete conversion of CO. Therefore, H₂ should also be able to promote NO oxidation for a NO/O₂/CO mixture by eliminating inhibition effects of CO. Although H₂ lowers the light-off temperature for CO oxidation, the activity for NO oxidation below 130°C is negligible (Figure 9.1a) which makes the effect of H₂ to enhance NO₂ yield in a NO/O₂/CO mixture become less prominent.

The TPR results with NO/O₂/CO/C₃H₆ (Figure 9.1d) showed that the addition of a low concentration of H₂ such as 250 ppm appeared to be beneficial for NO oxidation with respect to the light-off temperature as well as the NO₂ yield over the entire temperature range. Therefore, it can be suggested that the addition of about 250 ppm of H₂ is optimal to enhance the NO₂ yield for this complete DOC gas mixture. Higher H₂ concentrations were however found to lower the NO₂ yield for the temperature range of 250-400°C. The detrimental effect of increasing H₂ concentration at these higher temperatures was probably due to NO₂ consumption by H₂.

Chapter 10

Conclusions and outlook

The overall focus of this work is to increase understanding of the mechanisms of the H₂ effect on HC-SCR and DOC from lab-scale studies. Two types of catalyst namely Ag-Al₂O₃ and Pt/Al₂O₃ were used as model catalysts for HC-SCR and DOC, respectively. A combination of experimental measurements and kinetic modeling approaches were utilized as a way to examine mechanistic effects of H₂ for both catalysts.

NO oxidation to NO₂ has been suggested as a subsystem within the HC-SCR reaction network over Ag/Al₂O₃. **Paper I** demonstrated the role of H₂ to modify surface NO_x species during NO oxidation and C₃H₆-SCR over Ag-Al₂O₃ catalyst. TPD results suggested formations of two general groups of surface NO_x species: a less thermally stable group of so called “LT nitrates” and a more thermally stable group of “HT nitrates”. LT nitrate species were more likely related to the formation of inhibiting nitrate species on active sites. Feeding of H₂ was found to eliminate the LT nitrate and subsequently promoted the NO oxidation and C₃H₆-SCR. In addition, the presence of H₂ also promoted the formation of a greater variety of adsorbed hydrocarbons. As a result, it suggested that H₂ caused other effects to promote C₃H₆-SCR over Ag-Al₂O₃. It was also found that H₂ facilitated the formation of nitrate species mainly on the Al₂O₃ support. It was also indicative that the mechanism of NO_x storage on the Al₂O₃ support was mainly via NO₂ readsorption.

Paper II is focused on describing the promotional effect of H₂ on NO oxidation by a single role of H₂ to remove strongly adsorbed nitrate species on the active sites. A microkinetic model to describe a set of transient data based on a factorial design was constructed. A single type of active site was used to simplify the microkinetic model. A reaction network based on the Langmuir-Hinshelwood mechanism was proposed and it showed that the modeling results could capture well the experimental results.

A kinetic model for H₂-assisted C₃H₆-SCR over Ag-Al₂O₃ catalyst was developed in **Paper III**. The model was based on dual roles of H₂ to remove strongly adsorbed nitrates and simultaneous formation of more active Ag sites. The SCR reaction on the newly formed sites i.e. reduced Ag sites, was more rapid as reflected by significantly lower activation energy.

From experimental observations, a substantial amount of NO_2 formation was observed under both H_2 -assisted NO oxidation and H_2 -assisted C_3H_6 -SCR. However, in the absence of NO_x , addition of H_2 did not promote the C_3H_6 oxidation reaction. For the SCR feed mixture, H_2 was found to promote C_3H_6 oxidation. Whereas in the absence of H_2 , it appeared that the presence of NO_x inhibited C_3H_6 oxidation. The model could effectively capture a wide range of feed concentrations and temperatures, including temperature programmed experiments and transient experiments. From statistical analyses, all fitted kinetic parameters were found to be significant within 95% confidence intervals. Evaluation of mass transfer resistance in the washcoat indicated that during H_2 -assisted C_3H_6 -SCR, a mild influence from internal mass transfer for NO could be considered important already at 250°C . However, a larger fraction of experimental data was free from the influence of mass transport resistances.

As a continuation of studies, the use of TPD for surface species quantification to support a kinetic model, as presented in Chapter 8, will be of interest. This concept will test the applicability of TPD as a way to probe nitrate species on the catalyst. In addition, modeling of H_2 effects to induce NO_x storage over $\text{Ag}/\text{Al}_2\text{O}_3$ support will be advantageous to investigate the possibility to use $\text{Ag}/\text{Al}_2\text{O}_3$ catalysts in NO_x storage and reduction (NSR) processes.

A follow up study involving the DRIFT-MS technique to relate the changes in surface species with gas phase can be a potential route to enhance understanding of the HC-SCR mechanism. Chansai et al.[68] have highlighted the importance of short time contact to be able to identify reactive surface species and minimize their interference from spectator surface species. Repeated fast cycling with H_2 pulsing has been carried out recently by Kim et al. [74] showing effects on the NO_x conversion over two different time scales as a function of cycle time owing possibly to slow morphological changes in silver sites and other faster kinetic effects. Further clarification and verification by which H_2 modifies surface species formation, combined with morphological changes over $\text{Ag}-\text{Al}_2\text{O}_3$, can be an interesting direction for further studies to improve our understanding of HC-SCR over $\text{Ag}-\text{Al}_2\text{O}_3$ catalyst.

Paper IV focuses on the evaluation of H_2 effects on NO oxidation over $\text{Pt}/\text{Al}_2\text{O}_3$ using 4 gas mixtures: NO/O_2 , $\text{NO}/\text{O}_2/\text{CO}$, $\text{NO}/\text{O}_2/\text{C}_3\text{H}_6$ and $\text{NO}/\text{O}_2/\text{CO}/\text{C}_3\text{H}_6$. Formation of Pt oxide is known to deactivate NO oxidation which is a slow process occurring over the scale of several minutes. The results from TPR with NO/O_2 and $\text{NO}/\text{O}_2/\text{CO}$ mixtures showed that H_2 promoted the NO_2 yield in the temperature range of $200\text{-}300^\circ\text{C}$. H_2 was proposed to retard Pt oxide formation mainly at low temperatures (below ca. 200°C) which gave a temporal increase in NO_2 yield. For steady operation at higher temperatures with complete conversion of H_2 , Pt oxide formation was unaffected by H_2 . Additionally, it also appeared that CO played a role to retard low temperature Pt oxide formation which gave higher NO_2 yield in the absence of H_2 .

The interaction of H₂ to influence C₃H₆ and CO inhibition effects on the NO oxidation reaction was also investigated. For NO oxidation in C₃H₆ containing mixtures, it was evident that the promotional role of H₂ was to weaken the inhibition effect of C₃H₆ by lowering the light-off temperature for C₃H₆ oxidation. In addition, it has been widely reported in literature that H₂ promotes the oxidation of CO which thus may also promote NO oxidation. However, with low CO feed concentration such as 200 ppm used in **Paper IV**, CO was found to have only a weak inhibition effect on NO oxidation. From the interaction between CO and C₃H₆, it was found that CO has only a weak inhibition effect on C₃H₆ oxidation.

Transient experiments involving in/out switching of H₂ were conducted with all gas mixtures at 230°C. Upon introduction of H₂, the time response of H₂ and NO₂ signals as well as the catalyst temperature was used to discriminate between the heat and chemical effects. For C₃H₆ containing mixtures, it was found that the time response of the increase in the NO₂ signal was faster than the increase in catalyst temperature which indicated that H₂ had an effect on the catalytic surface chemistry to promote NO oxidation. The effects of H₂ can be related to a decreased blocking effect of adsorbed C₃H₆ species and prevention of the reaction of C₃H₆ with NO₂ to form NO.

For future studies, it is of interest to develop a kinetic model to gain a deeper understanding of the mechanism of the H₂ effects on Pt/Al₂O₃. For model construction, the model could start from simulating the H₂ effects on DOC mixtures with and without C₃H₆, from the results presented in **Paper IV**. A model for Pt catalysts can be a useful reference especially if there is an interest to extend the investigation of H₂ effects to bimetallic Pt-Pd DOC catalysts.

Acknowledgements

Taking a PhD degree is a long journey with many ups and downs in every turn. I have been fortunate to have great support from people around me during this journey. They have contributed in direct or indirect ways during my unforgettable stay at Chalmers.

My heartfelt acknowledgement goes to my main supervisor, Prof. Derek Creaser. I am heartily thankful to Derek whose encouragements, valuable comments, great supervision in every step of my PhD process. The good seeds you planted will always be the source of inspiration to me.

My co-supervisor Assoc. Prof. Hanna Härelind from Competence Centrum for Catalysis (KCK) is greatly acknowledged for her constant support, invaluable inputs throughout my PhD research.

I would also like to thank my examiner Prof. Bengt Andersson, especially for always being enthusiast about Indonesia. I would also thank the head Division of Chemical Engineering, Prof. Louise Olsson for great collaboration work. Prof. Claes Niklasson is greatly acknowledged for introducing me to Sweden and facilitated my master study at Chalmers several years ago. I would also like to thank Prof. Magnus Skoglundh of KCK to create a nice scientific atmosphere in KCK that inspired me. I also would like to thank Marianne Sognell and Malin Larsson for good administrative support.

My buddy Xavier Auvray, thanks for small and big things that we have shared together. I would also thank Nadia and Stanislava for great friendship during our time at Chalmers. I thank my past office mate Dr. Carolin Wang-Hansen and currently Dr. Chaoquan Hu for setting up a pleasant atmosphere and great tolerance in our office. I would also like to express my gratitude to Dr. Hannes Kannisto and Dr. Fredrik Gunnarsson for invaluable help in catalyst preparation. Björn Lundberg is greatly acknowledged for practical help with Matlab. Special thanks to silver alumina members at KCK for pleasant discussions and knowledge sharing. Thanks to all colleagues at the Division of Chemical Engineering and KCK Chalmers for pleasant working atmosphere. Sorry that I am not able to mention you all here.

I would also like to thank Indonesian friends in Göteborg known as *Laskar Göteborg*. I am destined to meet many Indonesian students here from various generations. Thanks for joy and funny things in every gathering. Special thanks to Ibrahim Rohman's family for sharing nice times in Göteborg. I always enjoyed all conversations with Indonesian PhD gang: Kurnia, Ferry and Erwin. *Good luck with the PhD!* I am also grateful to the Department of Chemical Engineering at Gadjah Mada University, Yogyakarta and all colleagues there for always being supportive for my postgraduate study in Sweden.

In a more personal level, I would like to thank my families: Badaruddin family (Yogyakarta) as well as Zulnasri Zubir family (Bontang) for their endless prayers and continuous support to me and my wife especially when we are far from home. Eventually, my ultimate gratitude goes to my wife Afrina and my children Ghaisani and Thariq for their true love and inspiration. My heart loves you.

The financial support from the Swedish Energy Agency and Swedish Research Council were gratefully acknowledged. This work was performed within the Competence Centre for Catalysis, which is hosted by Chalmers University of Technology and financially supported by the Swedish Energy Agency and the member companies AB Volvo, ECAPS AB, Haldor Topsøe A/S, Scania CV AB, Volvo Car Corporation AB and Wärtsilä Finland Oy.

References

- [1] T. Johnson, SAE Int. J. Engines 4 (2011) 143-157.
- [2] W.A. Majewski, What Are Diesel Emissions, www.dieselnet.com (accessed Dec 18th, 2014), 2012.
- [3] C.A.T. Center, Technical Bulletin: Nitrogen Oxides (NO_x), Why and How They Are Controlled, US Environmental Protection Agency Research Triangle Park, NC, 1999.
- [4] G.T. Miller, Living in the Environment: Principles, Connections and Solutions, Thomson Brooks/Cole, Toronto, Ontario Canada, 2007.
- [5] M.K. Khair, H. Jääskeläinen, Emission Formation in Diesel Engines, www.dieselnet.com (accessed on Dec 18th, 2014), 2008.
- [6] R.M. Heck, Farrauto R. J., Gulati, S.T., Catalytic Air Pollution Control: commercial technology, John Wiley & Sons, Hoboken, N.J., 2009.
- [7] S.i. Matsumoto, Catal. Today 29 (1996) 43-45.
- [8] L. Olsson, Fundamental Studies of Catalytic NO_x removal, Department of Chemical Reaction Engineering, Chalmers University of Technology, Gothenburg, 2002.
- [9] W.A. Majewsky, Diesel Oxidation Catalyst, www.dieselnet.com (accessed on Dec 18th, 2014), 2012.
- [10] W.A. Majewski, Diesel Particulate Matter, www.dieselnet.com (accessed Dec 18th, 2014), 2013.
- [11] A. Russell, W.S. Epling, Catal. Rev. 53 (2011) 337-423.
- [12] D. Bhatia, R.W. McCabe, M.P. Harold, V. Balakotaiah, J. Catal. 266 (2009) 106-119.
- [13] L. Olsson, E. Fridell, J. Catal. 210 (2002) 340-353.
- [14] K. Hauff, H. Dubbe, U. Tuttlies, G. Eigenberger, U. Nieken, Appl. Catal. B: Environ. 129 (2013) 273-281.
- [15] K. Hauff, U. Tuttlies, G. Eigenberger, U. Nieken, Appl. Catal. B: Environ. 123–124 (2012) 107-116.
- [16] P. Denton, A. Giroir-Fendler, H. Praliaud, M. Primet, J. Catal. 189 (2000) 410-420.
- [17] X. Auvray, T. Pingel, E. Olsson, L. Olsson, Appl. Catal. B: Environ. 129 (2013) 517-527.
- [18] S. Benard, L. Retailleau, F. Gaillard, P. Vernoux, A. Giroir-Fendler, Appl. Catal. B: Environ. 55 (2005) 11-21.
- [19] L. Olsson, B. Westerberg, H. Persson, E. Fridell, M. Skoglundh, B. Andersson, J. Phys. Chem. B 103 (1999) 10433-10439.
- [20] M. Al-Harbi, R. Hayes, M. Votsmeier, W.S. Epling, Can. J. Chem. Eng. 90 (2012) 1527-1538.
- [21] M. Irfan, J. Goo, S. Kim, Environmentalist 31 (2011) 4-10.
- [22] J.M. Herreros, S.S. Gill, I. Lefort, A. Tsolakis, P. Millington, E. Moss, , Appl. Catal. B: Environ. 147 (2014) 835-841.
- [23] H. Hamada, M. Haneda, Appl. Catal. A: Gen. 421–422 (2012) 1-13.
- [24] M. Sun, E.B. Croiset, R.R. Hudgins, P.L. Silveston, M. Menzinger, Ind. Eng. Chem. Res. 42 (2002) 37-45.

- [25] S. Salomons, M. Votsmeier, R.E. Hayes, A. Drochner, H. Vogel, J. Gieshof, *Catal. Today* 117 (2006) 491-497.
- [26] S.R. Katare, P.M. Laing, *SAE Int. J. Fuels Lubr.* 2 (2009-01-1268) 605-611.
- [27] S. Salomons, R.E. Hayes, M. Votsmeier, *Appl. Catal. A: Gen.* 352 (2009) 27-34.
- [28] W. Hauptmann, M. Votsmeier, H. Vogel, D.G. Vlachos, *Appl. Catal. A: Gen.* 397 (2011) 174-182.
- [29] N.D. Hoyle, P. Kumarasamy, V.A. Self, P.A. Sermon, M.S.W. Vong, *Catal. Today* 47 (1999) 45-49.
- [30] N. Rankovic, A. Nicolle, D. Berthout, P. Da Costa, *J. Phys. Chem. C* 115 (2011) 20225-20236.
- [31] L. Olsson, M. Abul-Milh, H. Karlsson, E. Jobson, P. Thormählen, A. Hinz, *Top. Catal.* 30-31 (2004) 85-90.
- [32] R. Lanza, E. Eriksson, L.J. Pettersson, *Catal. Today* 147 (2009) S279-S284.
- [33] M. Iwamoto, H. Yahiro, *Catal. Today* 22 (1994) 5-18.
- [34] W. Held, A. König, T. Richter, L. Puppe, *SAE Technical Publications Paper* 900496 (1990).
- [35] R. Burch, J.P. Breen, F.C. Meunier, *Appl. Catal. B: Environ.* 39 (2002) 283-303.
- [36] Z. Chajar, P. Denton, F. Berthet de Bernard, M. Primet, H. Praliaud, *Catal. Lett.* 55 (1998) 217-222.
- [37] H.-Y. Chen, W.M.H. Sachtler, *Catal. Today* 42 (1998) 73-83.
- [38] T. Miyadera, *Appl. Catal. B: Environ.* 2 (1993) 199-205.
- [39] S. Satokawa, Shibata, J., Shimizu, K.-i., Satsuma, A., Hattori, T., *Appl. Catal. B: Environ.* 42 (2003) 179-186.
- [40] J.P. Breen, R. Burch, *Top. Catal.* 39 (2006) 53-58.
- [41] S. Erkfeldt, A. Palmqvist, M. Petersson, *Top. Catal.* 54 (2011) 1219-1223.
- [42] K.-i. Shimizu, A. Satsuma, T. Hattori, *Appl. Catal. B: Environ.* 25 (2000) 239-247.
- [43] K.-i. Shimizu, A. Satsuma, *Phys. Chem. Chem. Phys.* 8 (2006) 2677-2695.
- [44] H. Kannisto, K. Arve, T. Pingel, A. Hellman, H. Harelind, K. Eranen, E. Olsson, M. Skoglundh, D.Y. Murzin, *Cat. Sci. Technol.* 3 (2013) 644-653.
- [45] K. Arve, J.R.H. Carucci, K. Eränen, A. Aho, D.Y. Murzin, *Appl. Catal. B: Environ.* 90 (2009) 603-612.
- [46] V. Houel, P. Millington, R. Rajaram, A. Tsolakis, *Appl. Catal. B: Environ.* 77 (2007) 29-34.
- [47] H. He, X.L. Zhang, Q. Wu, C.B. Zhang, Y.B. Yu, *Catal. Surv. Asia* 12 (2008) 38-55.
- [48] V. Houel, P. Millington, R. Rajaram, A. Tsolakis, *Appl. Catal. B: Environ.* 73 (2007) 203-207.
- [49] S. Tamm, H. Ingelsten, M. Skoglundh, A.C. Palmqvist, *Top. Catal.* 52 (2009) 1813-1816.
- [50] S. Kameoka, Y. Ukisu, T. Miyadera, *Phys. Chem. Chem. Phys.* 2 (2000) 367-372.
- [51] W.L. Johnson II, G.B. Fisher, T.J. Toops, *Catal. Today* 184 (2012) 166-177.
- [52] M. Männikkö, M. Skoglundh, H. Härelind, *Catal. Today*. DOI:10.1016/j.cattod.2014.11.029
- [53] S. Chansai, R. Burch, C. Hardacre, D. Norton, X. Bao, L. Lewis, *Appl. Catal. B: Environ.* 160-161 (2014) 356-364.
- [54] <http://www.bloomberg.com/apps/news?pid=newsarchive&sid=aoTA4CoaYPtk>, GE Announces Breakthrough Result on Hydrocarbon Lean NOx (accessed on Dec 31st, 2014), 2010.

- [55] N. Bogdanchikova, F.C. Meunier, M. Avalos-Borja, J.P. Breen, A. Pestryakov, *Appl. Catal. B: Environ.* 36 (2002) 287-297.
- [56] S.T. Korhonen, A.M. Beale, M.A. Newton, B.M. Weckhuysen, *J. Phys. Chem. C* 115 (2011) 885-896.
- [57] K.-i. Shimizu, K. Sawabe, A. Satsuma, *Cat. Sci. Technol.* 1 (2011) 331-341.
- [58] H. Kannisto, H.H. Ingelsten, M. Skoglundh, *J. Mol. Catal. A: Chem.* 302 (2009) 86-96.
- [59] J.P. Breen, R. Burch, C. Hardacre, C.J. Hill, C. Rioche, *J. Catal.* 246 (2007) 1-9.
- [60] K. Eränen, F. Klingstedt, K. Arve, L.E. Lindfors, D.Y. Murzin, *J. Catal.* 227 (2004) 328-343.
- [61] M. Yamaguchi, I. Goto, Z.M. Wang, M. Kumagai, *Stud. Surf. Sci. Catal.* 121 (1999) 371-374.
- [62] S. Chansai, R. Burch, C. Hardacre, J. Breen, F. Meunier, *J. Catal.* 276 (2010) 49-55.
- [63] S. Kameoka, T. Chafik, Y. Ukisu, T. Miyadera, *Catal. Lett.* 55 (1998) 211-215.
- [64] F. Thibault-Starzyk, E. Seguin, S. Thomas, M. Daturi, H. Arnolds, D.A. King, *Science* 324 (2009) 1048-1051.
- [65] S. Satokawa, *Chemistry Letters* (2000) 294-295.
- [66] J. Shibata, Y. Takada, A. Shichi, S. Satokawa, A. Satsuma, T. Hattori, *J. Catal.* 222 (2004) 368-376.
- [67] J. Shibata, K.-i. Shimizu, S. Satokawa, A. Satsuma, T. Hattori, *Phys. Chem. Chem. Phys.* 5 (2003) 2154-2160.
- [68] S. Chansai, R. Burch, C. Hardacre, J. Breen, F. Meunier, *J. Catal.* 281 (2011) 98-105.
- [69] D. Creaser, H. Kannisto, J. Sjöblom, H.H. Ingelsten, *Appl. Catal. B: Environ.* 90 (2009) 18-28.
- [70] R. Brosius, K. Arve, M.H. Grootaert, J.A. Martens, *J. Catal.* 231 (2005) 344-353.
- [71] K. Arve, H. Backman, F. Klingstedt, K. Eränen, D.Y. Murzin, *Appl. Catal. A: Gen.* 303 (2006) 96-102.
- [72] H. Kannisto, H.H. Ingelsten, M. Skoglundh, *Top. Catal.* 52 (2009) 1817-1820.
- [73] P. Sazama, L. Capek, H. Drobna, Z. Sobalik, J. Dedecek, K. Arve, B. Wichterlova, *J. Catal.* 232 (2005) 302-317.
- [74] P.S. Kim, M.K. Kim, B.K. Cho, I.S. Nam, S.H. Oh, *J. Catal.* 301 (2013) 65-76.
- [75] N. Sadokhina, D. Doronkin, P. Pributkov, V. Bukhtiyarov, R. Kvon, A. Stakheev, *Top. Catal.* 54 (2011) 1190-1196.
- [76] M. Richter, R. Fricke, R. Eckelt, *Catal. Lett.* 94 (2004) 115-118.
- [77] B. Lindström, J.A.J. Karlsson, P. Ekdunge, L. De Verdier, B. Häggendal, J. Dawody, M. Nilsson, L.J. Pettersson, *Int. J. Hydrogen Energ.* 34 (2009) 3367-3381.
- [78] H. Kannisto, X. Karatzas, J. Edvardsson, L.J. Pettersson, H.H. Ingelsten, *Appl. Catal. B: Environ.* 104 (2011) 74-83.
- [79] X. Auvray, *Fundamental studies of catalytic systems for diesel emission control*, Department of Chemical and Biological Engineering, Chalmers University of Technology, Göteborg, 2013.
- [80] J.W. Niemantsverdriet, *Spectroscopy in catalysis: an introduction*, Wiley-VCH Verlag GmbH & Co. KGaA, Weinheim, 2007.
- [81] J.W. Thybaut, G.B. Marin, *Kinetics of Catalyzed Reactions-Heterogeneous*, in: I.T. Horváth (Ed.), *Encyclopedia of Catalysis*, John Wiley & Sons, Inc., 2010.

- [82] J.A. Dumesic, D.F. Rudd, L.M. Aparicio, J.E. Rekoske, A.A. Treviño, *The microkinetics of heterogeneous catalysis*, ACS, Washington, D.C., 1993.
- [83] J. Sjöblom, *Parameter estimation in heterogeneous catalysis*, Department of Chemical and Biological Engineering, Chalmers University of Technology, Gothenburg, 2009.
- [84] I. Chorkendorff, J.W. Niemantsverdriet, *Concepts of Modern Catalysis and Kinetics*, Wiley-VCH Verlag GmbH & Co. KGaA, Weinheim, 2003.
- [85] K. Reuter, *Modeling and Simulation of Heterogeneous Catalytic Reactions*, 2011, pp. 71-111.
- [86] A.B. Mhadeshwar, B.H. Winkler, B. Eiteneer, D. Hancu, *Appl. Catal. B: Environ.* 89 (2009) 229-238.
- [87] H.S. Fogler, Chapter 14 in *Elements of Chemical Reaction Engineering 4th edition ed.*, Prentice Hall PTR, Westford, 2006.
- [88] R. Hawthorne, *AIChE Symp. Ser.* 70, 1974, p. 428.
- [89] G.F. Froment, K.B. Bischoff, J. De Wilde, *Chemical Reactor Analysis and Design 3rd edition*, John Wiley & Sons, New York, 2010.
- [90] E.N. Fuller, P.D. Schettler, J.C. Giddings, *Ind. Eng. Chem.* 58 (1966) 18-27.
- [91] D.D. Do, *Adsorption analysis: equilibria and kinetics*, Imperial College Press, London, 1998.
- [92] Y. Guo, J. Chen, H. Kameyama, *Appl. Catal. A: Gen.* 397 (2011) 163-170.
- [93] U. Bentrup, M. Richter, R. Fricke, *Appl. Catal. B: Environ.* 55 (2005) 213-220.
- [94] Y. Guo, M. Sakurai, H. Kameyama, *Appl. Catal. B: Environ.* 79 (2008) 382-393.
- [95] X. She, M. Flytzani-Stephanopoulos, *J. Catal.* 237 (2006) 79-93.
- [96] S. Klacar, A. Hellman, I. Panas, H. Grönbeck, *J. Phys. Chem. C* 114 (2010) 12610-12617.
- [97] X. Zhang, H. He, H. Gao, Y. Yu, *Spectrochim. Acta Part A* 71 (2008) 1446-1451.
- [98] S. Tamm, N. Vallim, M. Skoglundh, L. Olsson, *J. Catal.* 307 (2013) 153-161.
- [99] H. Härelind, F. Gunnarsson, S.M.S. Vaghefi, M. Skoglundh, P.A. Carlsson, *ACS Catal.* 2 (2012) 1615-1623.
- [100] J.H. Lee, S.J. Schmiegel, S.H. Oh, *Appl. Catal. A: Gen.* 342 (2008) 78-86.
- [101] F.C. Meunier, V. Zuzaniuk, J.P. Breen, M. Olsson, J.R.H. Ross, *Catal. Today* 59 (2000) 287-304.
- [102] R. Burch, J.P. Breen, C.J. Hill, B. Krutzsch, B. Konrad, E. Jobson, L. Cider, K. Eränen, F. Klingstedt, L.E. Lindfors, *Top. Catal.* 30-31 (2004) 19-25.
- [103] H. Backman, K. Arve, F. Klingstedt, D.Y. Murzin, *Appl. Catal. A: Gen.* 304 (2006) 86-92.
- [104] H. Backman, J. Jensén, F. Klingstedt, J. Wärnå, T. Salmi, D.Y. Murzin, *Appl. Catal. A: Gen.* 273 (2004) 303-307.
- [105] T.C. O'Haver, peakfit version 4.21. Retrieved from:
<http://www.mathworks.com/matlabcentral/fileexchange/23611-command-line-peak-fitting-function-for-time-series-signals>, 2013.
- [106] S. Tamm, S. Andonova, L. Olsson, *Catal. Lett.* 144 (2014) 674-684.
- [107] S. Tamm, S. Andonova, L. Olsson, *Catal. Lett.* 144 (2014) 1101-1112.
- [108] S. Ren, S.J. Schmiegel, C.K. Koch, G. Qi, W. Li, *Catal. Today*. DOI: 10.1016/j.cattod.2015.02.008

- [109] W. Hauptmann, M. Votsmeier, J. Gieshoff, A. Drochner, H. Vogel, *Appl. Catal. B: Environ.* 93 (2009) 22-29.
- [110] K. Irani, W.S. Epling, R. Blint, *Appl. Catal. B: Environ.* 92 (2009) 422-428.